AD-A181 618 HYPERVELOCITY OXYGEN SOURCE FOR THE STUDY OF ATOM-SURFACE INTERACTIONS(U) AERODYNE RESEARCH INC BILLERICA MA A FREEDMAN ET AL APR 87 ARI-RR-588 1/1

UNCLASSIFIED AFOSR-TR-87-0661 F49620-86-C-0091 F/G 7/4 NL

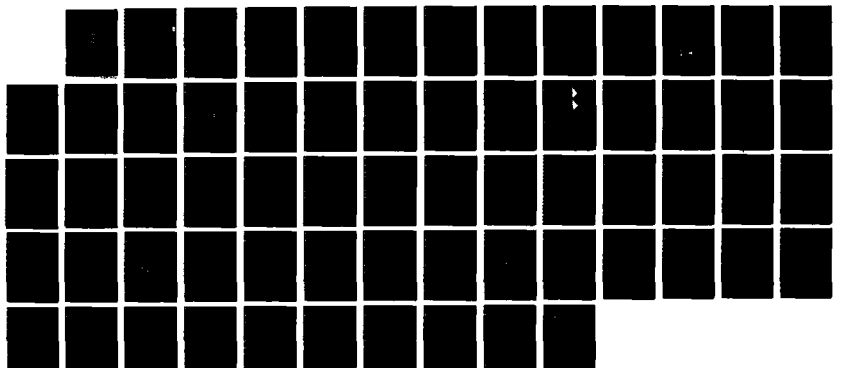

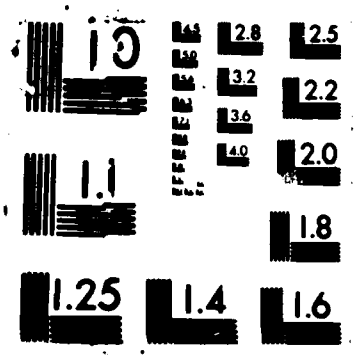
1.0
1.1
2.8
3.2
3.6
4.0
2.5
2.2
2.0
1.8
1.25
1.4
1.6

ARI-RR-588

AFOSR-TR- 87-0661

HYPERVELOCITY OXYGEN SOURCE FOR THE STUDY OF ATOM-SURFACE INTERACTIONS

Prepared by

Andrew Freedman and William Unkel
Aerodyne Research, Inc.
45 Manning Road
Billerica, MA 01821

Prepared for

Drs. Francis Wodarczyk and Larry Burggraf
Air Force Office of Scientific Research

Under Contract F49620-86-C-0091

April 1987

UNCLASSIFIED
SECURITY CLASSIFICATION OF THIS PAGE

AD-A181 618

REPORT DOCUMENTATION PAGE

1a. REPORT SECURITY CLASSIFICATION Unclassified	1b. RESTRICTIVE MARKINGS
2a. SECURITY CLASSIFICATION AUTHORITY	3. DISTRIBUTION/AVAILABILITY OF REPORT Distribution unlimited; approved for public release
2b. DECLASSIFICATION/DOWNGRADING SCHEDULE	
4. PERFORMING ORGANIZATION REPORT NUMBER(S) ARI-RR-588	5. MONITORING ORGANIZATION REPORT NUMBER(S) AFOSR-TR- 87-0661
6a. NAME OF PERFORMING ORGANIZATION Aerodyne Research, Inc. — 6b. OFFICE SYMBOL (If applicable)	7a. NAME OF MONITORING ORGANIZATION Air Force Office of Scientific Research
6c. ADDRESS (City, State, and ZIP Code) 45 Manning Road Billerica, MA 01821	7b. ADDRESS (City, State, and ZIP Code) Building 410 Bolling AFB, DC 20332-6448
8a. NAME OF FUNDING/SPONSORING ORGANIZATION AFOSR — 8b. OFFICE SYMBOL (If applicable) NC	9. PROCUREMENT INSTRUMENT IDENTIFICATION NUMBER F49620-86-C-0091
8c. ADDRESS (City, State, and ZIP Code) Bldg 410 Bolling AFB, DC 20332-6448	10. SOURCE OF FUNDING NUMBERS PROGRAM ELEMENT NO.: 61102F — PROJECT NO.: 3005 — TASK NO.: A1 — WORK UNIT ACCESSION NO.:

11. TITLE (Include Security Classification)
Hypervelocity Oxygen Source for the Study of Atom-Surface Interactions

12. PERSONAL AUTHOR(S)
Freedman, Andrew and Unkel, William

13a. TYPE OF REPORT	13b. TIME COVERED FROM	14. DATE OF REPORT (Year, Month, Day)	15. PAGE COUNT
Final		April 87	61

16. SUPPLEMENTARY NOTATION

17. COSATI CODES		
FIELD	GROUP	SUB-GROUP

18. SUBJECT TERMS (Continue on reverse if necessary and identify by block number)
Atomic oxygen beam source, nozzle source, gas-surface interactions

19. ABSTRACT (Continue on reverse if necessary and identify by block number)

Space-based facilities face an unexpectedly hostile environment at orbital altitudes due to chemical interaction with atomic oxygen at high velocities (typically 8 km/s). Shuttle-based experiments indicate substantial degradation and erosion of various materials which face into the atmospheric wind. This document reports the efforts of a Phase I SBIR project intended to design a high velocity, high flux atomic oxygen beam source capable of simulating the space environment. Also included are plans for a vacuum apparatus which will provide for the diagnostic techniques needed to evaluate the source performances as well as allow for materials testing.

The oxygen atom beam source is based on the concept of admixing a small quantity of molecular oxygen into a gas stream of helium that had been electric discharge heated using a commercially available plasma torch.

...continued...

20. DISTRIBUTION/AVAILABILITY OF ABSTRACT	21. ABSTRACT SECURITY CLASSIFICATION
☒ UNCLASSIFIED/UNLIMITED ☒ SAME AS RPT. ☐ DTIC USERS	Unclassified

22a. NAME OF RESPONSIBLE INDIVIDUAL	22b. TELEPHONE (Include Area Code)	22c. OFFICE SYMBOL
Dr. Frank Wodarczyk	(202) 767-4960	NC

DD FORM 1473, 84 MAR — 83 APR edition may be used until exhausted. All other editions are obsolete. — SECURITY CLASSIFICATION OF THIS PAGE

19. ABSTRACT (continued)

Extensive modeling has suggested improvements in a previous version of the source [Review of Scientific Instruments 53, 1714 (1982)] that should allow production of 8 eV s^{-1} beams with atomic oxygen fluxes of 1 x 10^{17} cm^{-2} s^{-1} at 10 cm distance from the source aperture. Metastable atom production should be minimal (10^{-3}). The major changes entail a new oxygen injection system and enlargement of the source aperture. This latter change requires the incorporation of a Campargue style "zone-of-silence" nozzle skimmer system in the vacuum apparatus in order to handle the increased gas load. Schematics of the redesigned source and vacuum apparatus as well as suggestions for future research are included.

Table of Contents

LIST OF ILLUSTRATIONS

List of Illustrations (Continued)

1. INTRODUCTION

1.1 Motivation

Space-based facilities face an unexpectedly hostile environment at orbital altitudes (between 100 and 500 km) due to chemical interaction with atomic oxygen at the high velocities of orbiting spacecraft (up to 8 km s^{-1}). Recent shuttle-based experiments indicate substantial degradation and erosion of various materials which face into the "atmospheric wind".[1-6] This effect could have profound implications for both the effective life and utility of satellites and space station systems. A further ramification is that surface degradation apparently produces direct optical interferences[7-12] as well as molecular off-gassing which can lead to significant contamination of space-based optical instrumentation.

Leger and Visentine[13] have reviewed the effects of Low Earth Orbit (LEO) on space station structural materials and have come to some startling conclusions. Based on two space shuttle flights (STS-5 and STS-8), they have established that carbon based composites, polymers and organic films have reaction efficiencies with oxygen atoms of 3×10^{-24} cm^3 $atom^{-1}$. When the apparent oxygen atom flux as a function of solar activity is folded into the calculation, they conclude that material surface erosion could reach 10-100 μm per year at 500 km altitude; at an altitude of 200 km (nominal space station orbit), 10 mm per year will be lost! Thus, over a 30 year anticipated lifetime for advanced space structures, structural integrity might be threatened by oxygen atom induced erosion.

Another consideration is the high velocity presented by the orbit of space structures. At 8 kms^{-1}, as mentioned before, space shuttle experiments have shown rapid material erosion; but at thermal velocities, experiments have indicated little or no reaction. Arnold, Peplinski and Cascarano have

concluded that there is a translational energy barrier to erosion, and that any test facility must produce hyperthermal oxygen atoms.[14]

DOD has need of a facility designed to study the effects of atomic oxygen on erosion and oxidation of the surfaces of sensitive materials. This laboratory apparatus would need to adequately simulate the space environment and contain state-of-the-art diagnostic instrumentation. The centerpiece of such a facility must be its atomic oxygen beam source which would be required to produce both a fast (6 - 8 km s^{-1}) and intense (10^{16} cm^{-2} s^{-1}) atomic oxygen beam. The former requirement is set by the speed of orbiting spacecraft and the sharp energy dependence of gas-surface interactions while the latter reflects a surface exposure 200 times greater than that faced by a spacecraft at 300 km altitude. Thus a year's exposure could be accomplished in a matter of two days.

From an academic standpoint, beam-surface interactions at moderate energies are an uncharted area of research. Chemists tend to study thermal processes ($T < 5000$ K) at average energies of less than 0.2 eV while physicists usually study keV ion beams. At 8 km s^{-1}, atomic oxygen or nitrogen beam contains enough energy to collisionally dissociate or vibrationally excite another molecule as well as sputter atoms off a surface. One might also expect new reactive mechanisms to appear at these energies. The aforementioned work by Arnold, Pelinski, and Cascarano[14] indicates that energy barriers of several electron volts preclude study of hydrocarbon reactions by conventional techniques. This source may be unique in producing these, intermediate energies (for light atoms and molecules) without substantial metastable contamination.

1.2 Background

Simulation of ambient space conditions places great constraints on atomic oxygen sources. First, the velocity of orbital spacecraft tends to be near 8 km s^{-1} which, for oxygen atoms, is equivalent to a thermal temperature of

~60,000 K. Second, the flux of oxygen atoms at these velocities and at an altitude of 300 km is approximately 3×10^{14} cm^{-2} s^{-1}. Thus, in order to simulate erosion and oxidation over a period of time, the source must produce very high fluxes of atomic oxygen at high energies (> 5 eV). A further constraint is the low pressure of space (< 10^{-6} torr); a realistic simulation would require the use of high vacuums and rule out high pressure thermal sources. What is required is a supersonic nozzle atomic oxygen beam source meeting the above characteristics.

The development of high intensity, variable velocity molecular beam sources of free radicals has been a goal of the chemical physics community for the past two decades. Previous approaches to atomic oxygen beam sources have been based on thermal dissociation, radio-frequency discharge, and microwave discharge techniques. Geddes, et al[15] thermally dissociated pure oxygen at 2100 K and low pressures (~1 Torr). Unfortunately, the dissociation efficiency (6 - 8%), velocity (1.5 km s^{-1}) and intensity were low. The efficiency of such a source is limited by the low pressures involved and the lack of materials able to withstand oxidation at higher temperatures. Sibener, et al[16] (based on the work of Miller and Patch[17]) used a high pressure RF discharge with argon and helium as carrier gases. While the oxygen atom fluxes are quite high in this source, the velocity range (1.25 - 2.25 km s^{-1}) is limited. Another significant drawback is the substantial presence of electronically excited oxygen atoms, which allow for elegant studies of chemical reactions,[18] but complicate energy transfer measurements. The results of Gorry, et al[19] using microwave techniques were similar to those obtained in the RF discharge sources.

Work at Aerodyne Research (ARI) has resulted in the first continuous high flux atomic oxygen source which produces an atomic beam approaching orbital velocities. The ARI designed source presented below derives from the work of Knuth and co-workers,[20] who developed an electrical arc discharge source which produced very high energy (up to 21 eV) beams of rare gases. Bickes, et al[21] later developed a similar source for producing nitrogen atoms by blending

molecular nitrogen into the rare gas flow. In both cases, however, significant production of excited state species was found. Moreover, a significant drawback in using these sources with oxygen is the rapid corrosion of the metal electrodes. We solved these problems by introducing oxygen as a minor constituent downstream of the discharge region. By providing a long channel before the beam is formed, most metastable or ionic species are quenched. If sufficient time is available, the resulting species distribution approaches that of high temperature equilibrium (~3000 - 7000 K), while the seeded supersonic expansion provides for an accelerated and narrow velocity distribution.

The ARI atomic oxygen source[22] consists of two parts, a commercial DC plasma torch (TAFA Corporation) and a beam-forming nozzle section constructed of OHFC copper. The torch is used to provide a source of high temperature inert gas at atmospheric pressure. The arc operates in a "non-transferred mode," meaning that the gas is heated as it passes through the discharge, which is contained entirely within the body of the torch. As illustrated in Figure 1, the oxygen is admixed 2 cm downstream of the discharge region

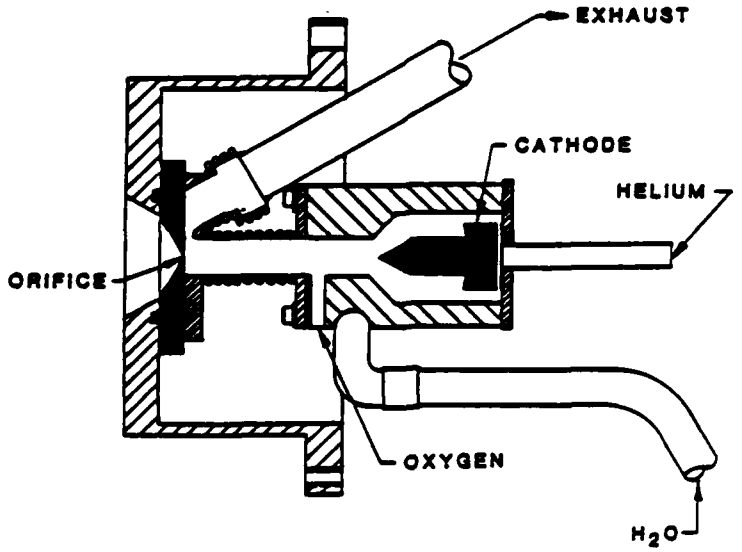

Figure 1. Schematic of Aerodyne-designed Atomic Oxygen Source

through an inlet originally intended for introduction of powder for spray deposition. The inlet diameter was reduced to 0.05 cm so that it acts as a sonic injector, providing rapid mixing of the oxygen with the carrier gas. The gas then flows down a 4 cm (0.80 cm diameter) channel in the nozzle section before encountering an annual chamber through which virtually all of the gas is exhausted. A small fraction flows through a 0.0125 cm diameter hole into the vacuum chamber, forming the molecular beam. The design of the nozzle section is such that it has no internal O-rings and the water-cooling and gas channels are completely separated. An earlier version of this source had a replaceable nozzle and a host of O-rings which led to repeated failures of the system. Because the nozzle hole did not deteriorate during normal operation as had been feared in the early designs, a replaceable nozzle piece was deemed unnecessary.

This initial design produced 4 km s^{-1} oxygen atom beams (see Figure 2) with approximately 30-40% oxygen dissociation. Further testing indicated that the basic approach was sound; the plasma torch could produce (if used at full power) gas temperatures of 7500 K and therefore, 100% dissociation and 8 km s^{-1} velocities. The problems lay in the aperture size (too small) and oxygen injection system (inefficient).

1.3 Phase I Technical Objectives

Phase I is the first step in a proposed multi-phase project to design, construct, and test a ground-based facility which provides for the study of the interactions of high velocity atomic oxygen and molecular nitrogen with space-based materials. The Phase I research centered on the redesign of the Aerodyne hypervelocity atomic oxygen beam source to allow production of higher velocities and higher fluxes. As a result of this redesign, the same source is now suitable for the production of molecular and atomic nitrogen beams (by rejecting N_2 rather than O_2), thus providing a source of other major components of the orbital altitude atmospheric flux. We have designed a beam source test facility which would incorporate a "zone of silence" skimmer as

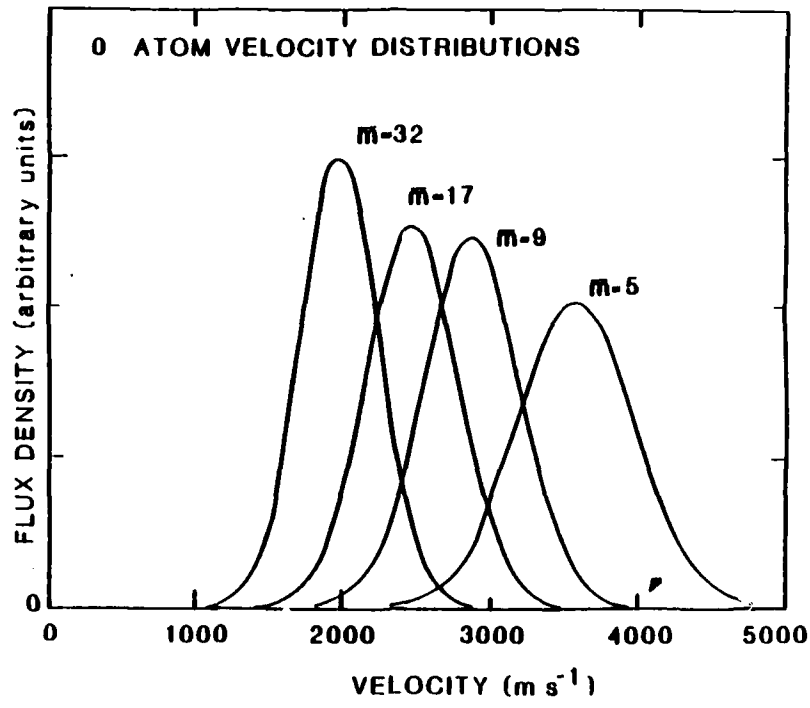

Figure 2. Velocity Distribution of Atomic Oxygen Beam As a Function of Average Mass of the Carrier Gas

developed by Campargue[23-25] which would greatly lessen the vacuum pumping requirements of such a system.

The Phase I technical objectives included:

- o Redesigning the Aerodyne hypervelocity atomic oxygen source to produce higher velocities and higher fluxes.
- o Designing a "zone of silence" nozzle-skimmer system for such a source in the manner of Campargue and,
- o Providing a schematic of a three chamber molecular beam system to be used in testing the hypervelocity source.

The Phase II project would include building the redesigned source and test chamber and testing the oxygen atom source. With the successful completion of

these tasks, an extremely sophisticated test facility based on the high flux fast atomic oxygen source and incorporating various surface diagnostic techniques would be straightforward to design and construct.

1.4 Phase I Summary

The results of the Phase I project can be summarized as follows:

- The oxygen injection system has been redesigned incorporating greater flexibility so as to allow proper mixing of the oxygen and hot carrier gas.
- The effect of aperture enlargement on the source performance has been modeled. Opening the aperture to a diameter of 0.5 mm will provide stagnation temperatures sufficient to produce an 8 km s^{-1} oxygen (or nitrogen) beam.
- A three chamber molecular beam apparatus has been designed to accommodate the Campargue nozzle-skimmer system and provide mass spectrometric determination of beam characteristics. The calculated flux of atomic oxygen at 10 cm distance from the source is 1.2 x 10^{17} cm^{-2} s^{-1}.

The rest of this report has been separated into three sections. Section 2 presents an effort (using modeling) to fully characterize the source and nozzle expansion process as well as provide the necessary design parameters for the vacuum system. Section 3 provides schematics and brief descriptions of the new atomic oxygen source and vacuum chamber. Section 4 provides a concluding summary as well as suggestions for future research.

2.0 MODELING EFFORTS

2.1 Introduction

We have divided the modeling effort into two distinct parts. The first involves the redesign of the Aerodyne oxygen-atom source so as to maximize velocity and flux. This work was performed by Professor Unkel. The second part, performed by Dr. Freedman, involved calculating the effects of using the redesigned source as part of a Campargue "zone-of-silence" nozzle-skimmer arrangement and the demands placed on its associated vacuum system. In addition, ultimate performance characteristics of the whole system were calculated. It must be stressed that the redesigned source and Campargue nozzle-skimmer arrangement must be considered as an integral whole.

The modeling effort to redesign the source stems from heat transfer measurements performed after publication of the paper in the Review of Scientific Instruments. The following conclusions about redesigning the source were reached:

1. The redesigned source could thermally withstand the highest power settings of the commercial plasma torch. The major improvement was use of higher water flow velocities through the various source parts. This was accomplished by using narrow channels and high pressures (produced by a booster pump capable of reaching 400 psi).

2. Bulk gas temperature of over 5000 K could be produced in helium (see Figure 4). At these temperatures, beam velocities of up to 7 km s^{-1} and oxygen dissociation efficiencies of 100% could be reached.

3. The simple injection system used in previous studies was not sufficient to properly mix the cold oxygen into the hot carrier gas. A more elaborate design using multiple injection ports pointed upstream constitutes a major improvement.

4. The problem of the nozzle aperture sampling a boundary layer of cold gas instead of the hot zone was not explicitly addressed by the present studies, but it is apparent that enlarging the aperture is the simplest solution.

Subsection 2.2 centers on the design of a proper oxygen injection system and the effects of enlarging the source aperture on the effective gas stagnation temperatures. Subsection 2.3 deals with the effects of higher temperatures and fluxes on the necessary vacuum system and Subsection 2.4 with the source performance itself.

2.2 Stagnation Conditions

The main oxygen source components are the plasma torch itself through which flows the "carrier" helium gas, the oxygen injection section, the mixing tube, the stagnation plate with the nozzle and the exhaust system (see Figure 3). Torch performance is characterized by the temperature of the gases at the inlet to the expansion nozzle. Also of key importance is the need to insure that oxygen injected at the start of the mixing tube has indeed mixed well and equilibrated with the main flow. The calculations performed include:

a. Penetration of the center of the oxygen jet(s) and entrainment of the oxygen into the main flow;

b. Determination of the bulk (average temperature) of the fluid at the exit of the mixing tube (making use of previous experimental data);

c. Estimation of the average temperature of the gas entering the expansion nozzle, including the effects of the end wall boundary layer; and

d. Comparison of computed results with previous experimental results where the average temperature was inferred.

A brief description of each calculation and the main results are given in the sections below. The calculations are somewhat inexact but as will be shown, they are in reasonable agreement with the previous experimental results.

A87-101

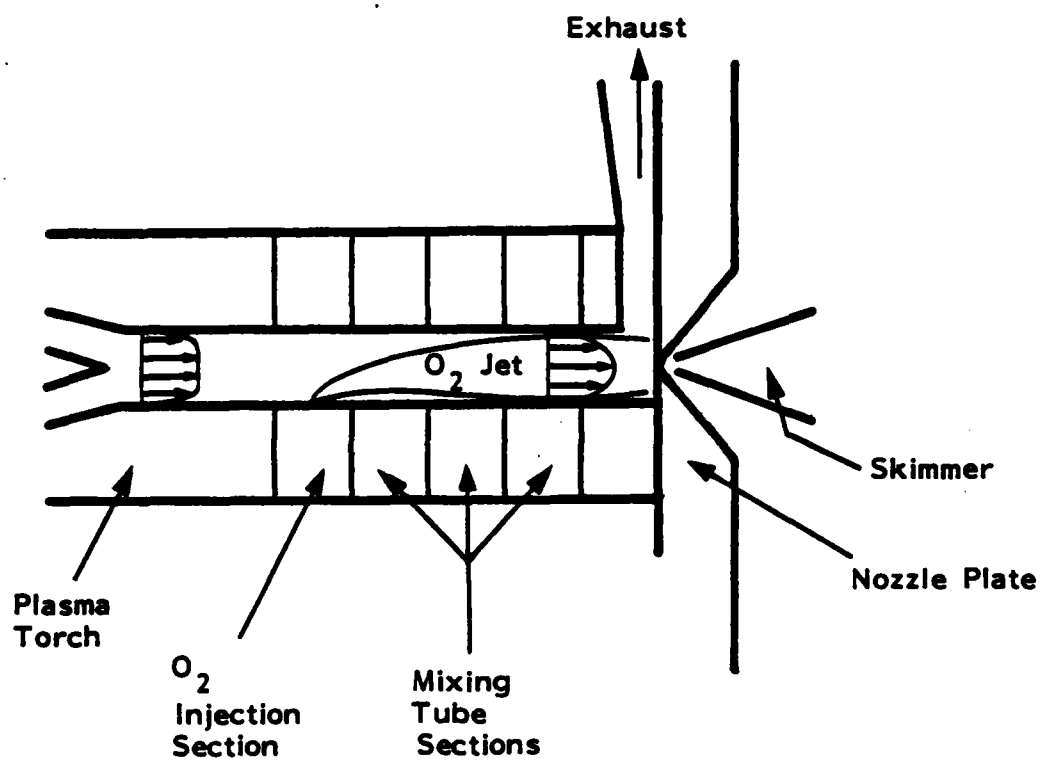

Figure 3. Schematic of O_2 Source Components

2.2.1 Oxygen Jet Penetration and Entrainment

The oxygen injection port size and number of ports must be designed to allow penetration of the jet to the center of the main flow and allow for good entrainment of the jet into the main flow. The overall situation is shown in Figure 4. To accommodate variations in oxygen fraction, the injector is designed with 4 injection ports, any of which can be blocked. The penetration results are summarized in Figure 5 where the position of the jet centerline is plotted as function of Oxygen % (molar), with the results shown for 1,2 and 4 of the holes open. In these calculations the behavior is computed based on the correct flow through each jet hole but the actual trajectory of the jet is computed as if only one jet were present. The calculations use the corrections of Abramovich[26] for mixing of a jet into a cross-stream.

The results shown are for all injection holes at a fixed diameter of 0.25 mm (10 mil). At 2% oxygen and with all 4 holes open, or at 1% oxygen and 2 holes open, the jet has penetrated to the tube centerline by the end of the

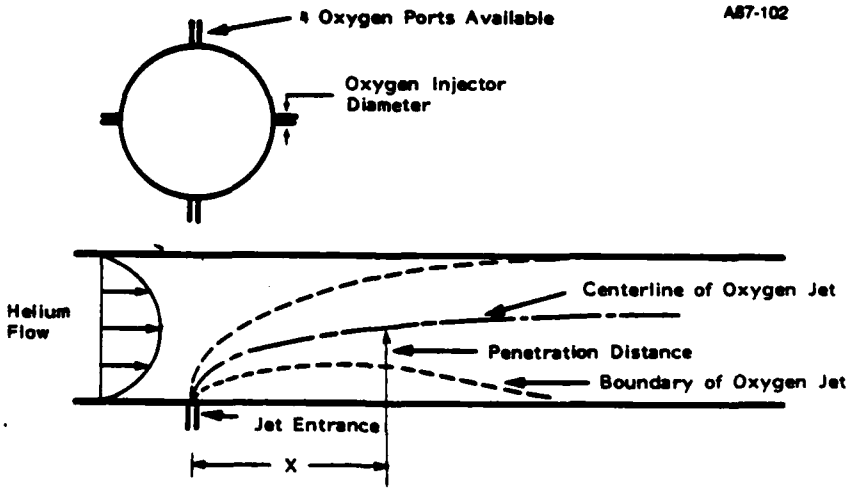

Figure 4. Schematic Showing Oxygen Mixing Region

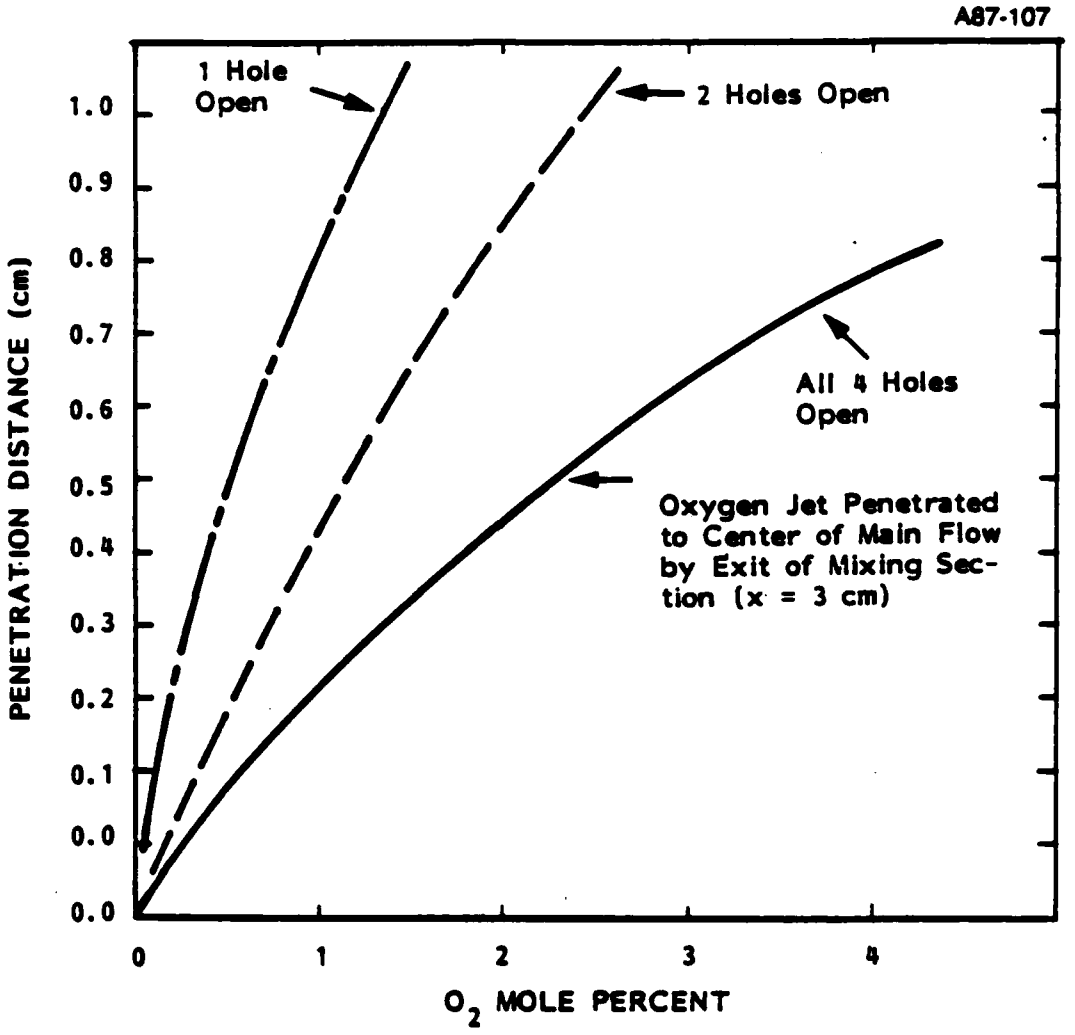

Figure 5. Penetration Distance Results With O_2 Injector Diameter at 0.25 mm

mixing tube. Neither the total flow rate (if oxygen fraction is fixed) nor the average temperature of the carrier gas will have a strong effect on the mixing characteristics.

The jet spreading is estimated roughly by considering a 12 degree included angle for mixing.[27] With this angle the jet will open up to about 84% of the flow channel diameter by the tube end (for tube radius/tube length ratio of 8).

Constraints of construction require that the injection holes be slanted rather than at a 90 degree angle to the main flow. The holes will be slanted to inject slightly upstream, improving the mixing and penetration somewhat.

The mixing tube is designed in sections and can be lengthened or shortened if necessary.

2.2.2 Calculation of Stagnation Temperature

Previous experimentation with the torch and mixing tube provide extensive data on the operating conditions including the torch/tube heat losses. In these experiments, the arc voltage and current were measured to determine the input power, and instrumented water cooling system measurements were used to determine the heat losses. From the losses, the bulk, or average temperature of the gas leaving the torch and leaving the tube can be determined. The results are summarized in Figure 6, where inferred temperature is plotted as a function of the torch and input power. Losses in the torch increase with increased helium flow as shown in the figure. However, the losses in the tube decrease as the flow rate increases with the net result that, for a tube length of approximately 3 cm, the bulk temperature at the tube output does not change significantly with helium flow rate. The experimental results indicate a roughly linear variation of bulk temperature with power input, with a bulk temperature of 4000 K at an electrical input of approximately 12 kW. Extrapolating to a power input of 20 kW would indicate that a bulk temperature of 6000 K can be achieved with the torch.

Estimate of Core Temperature

The experimental results give only the bulk temperature and it is necessary to estimate the temperature of the material that will enter the nozzle. The nozzle will collect fluid from the center of the main flow, where the temperature will be considerably greater than the average. At the lower flow rates, calculations indicate that the boundary layers formed along the tube wall will have met by the end of the mixing tube. At the highest flow rates run in the experiments, the boundary layers will fill 80% or more of the radius. Reasonable estimates can be made assuming that the flow is fully

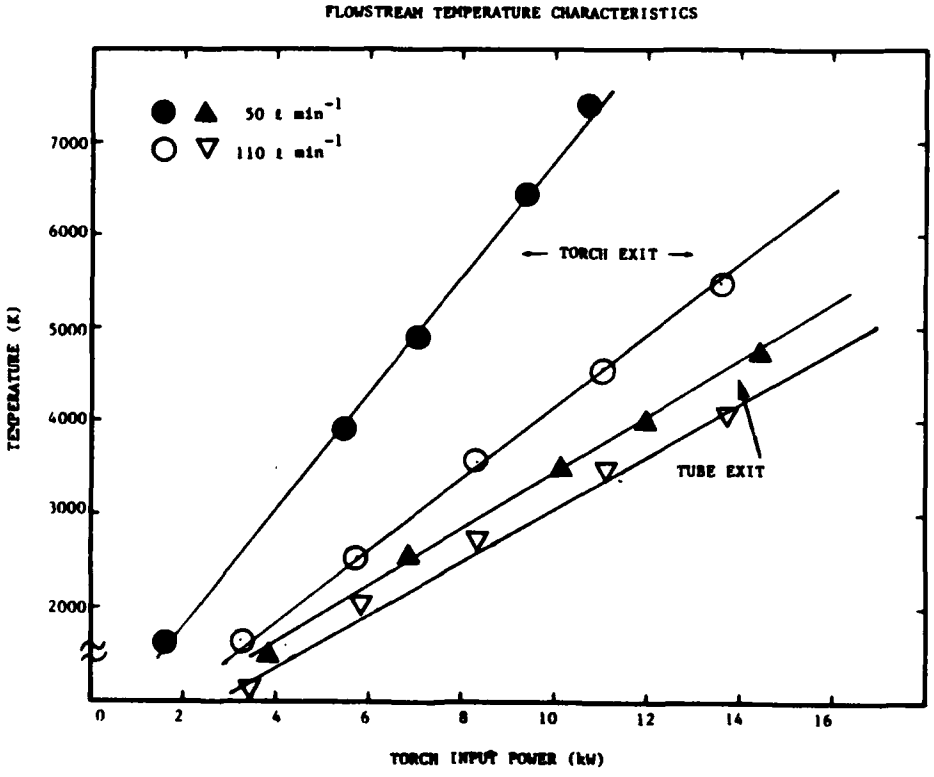

Figure 6. Flowstream Temperature Characteristics Derived from Thermal Load Testing

developed, and is laminar as indicated by the Reynolds number. For fully developed flow, the temperature profile will be roughly parabolic and the centerline temperature can be determined as

$$T(\text{centerline}) = T_{wall} + 2\,(T_{bulk} - T_{wall}) \quad . \qquad (1)$$

Assuming a wall temperature of 400 K, a bulk temperature of 4000 K corresponds to a centerline temperature of 7600 K and bulk temperature of 6000 K corresponds to a centerline temperature of 11600 K.

A somewhat more conservative estimate is to assume that the flow to the nozzle is collected from the center half radius, for which the average temperature can be found as

$$T(R/2)_{ave} = T_{wall} + 1.75\ (T_{bulk} - T_{wall}) \qquad (2)$$

These result in the effective nozzle plate temperatures as a function of torch power. At 16 kW input power, an effective temperature of 8500 K is achieved.

Note that the estimated convective heat losses of the tube underpredicted the measured losses, indicating that radiation losses are significant. Since the radiative losses will come preferentially from the center of the flow, radiation has the effect of flattening the temperature profile, and therefore decreasing the centerline temperature for a given average temperature. Thus the estimates given here may be somewhat high.

Average Temperature of the Gases Entering the Nozzle

The gas leaving the mixing tube is pushed against the nozzle plate in a stagnation type flow as shown in Figure 7. A boundary layer is formed along the nozzle plate, and some of the fluid drawn through the nozzle must pass through this boundary layer. The qualitative flow pattern is shown in Figure 7. A conservative estimate (that is, a low value) can be determined by first determining the 'capture' cylinder, that is the radius of the main flow that can provide the required flow to the nozzle hole. The flow rate through the nozzle can be determined from the nozzle diameter and the upstream conditions using the standard choked flow nozzle equations. Given this flow rate and the flow rate in the mixing tube, the 'capture' cylinder can be computed. The thickness of the boundary layer on the nozzle plate can be estimated using results for an axisymmetric laminar stagnation flow. The strength of the stagnation flow is computed from the velocity of the main flow.

For the situation where the boundary layer is smaller than the capture radius, a rough estimate is obtained by assuming that the fluid that comes

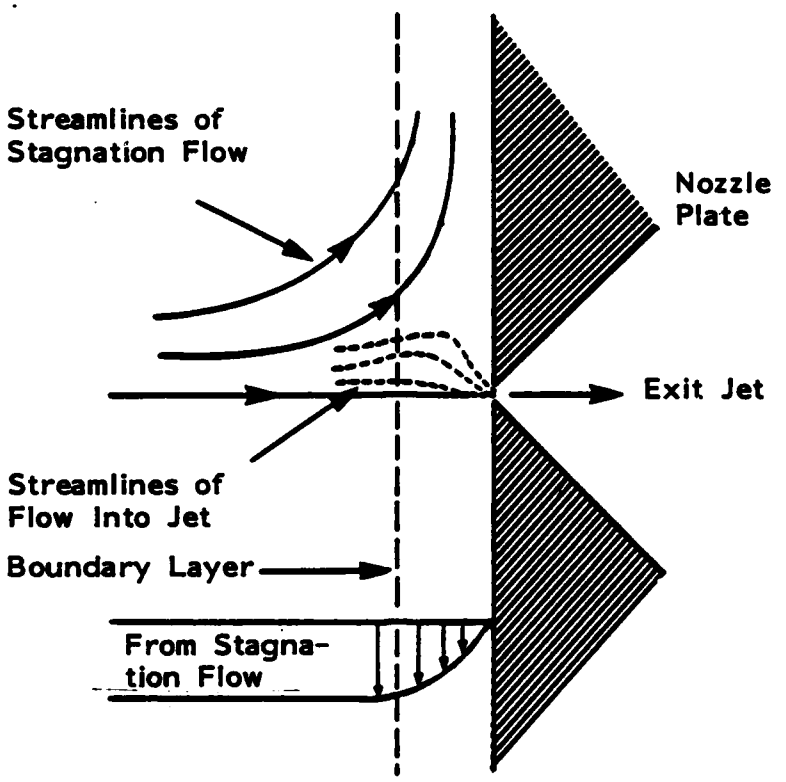

Figure 7. Schematic of Flow Near the Nozzle. A stagnation type flow is set up by the turning of the main flow. A sink type flow is setup by the nozzle itself.

from an outer annulus must pass through the boundary layer formed over the plate. The thickness of this outer ring is assumed to be equal to the boundary layer thickness. The fluid interior to this annulus does not pass through the boundary layer (See Figure 8b).

These estimates should err on the side of giving a low estimate for two reasons. First, the boundary layer will be thinned by the high speed fluid flow to the hole, and second, the fluid affected thermally by the wall will also be slowed. Therefore, there will be a tendency to draw more of the fluid from the region toward the center of the flow.

The calculated results are summarized in Figure 9 where the average temperature of the fluid entering the nozzle is plotted against the thermal

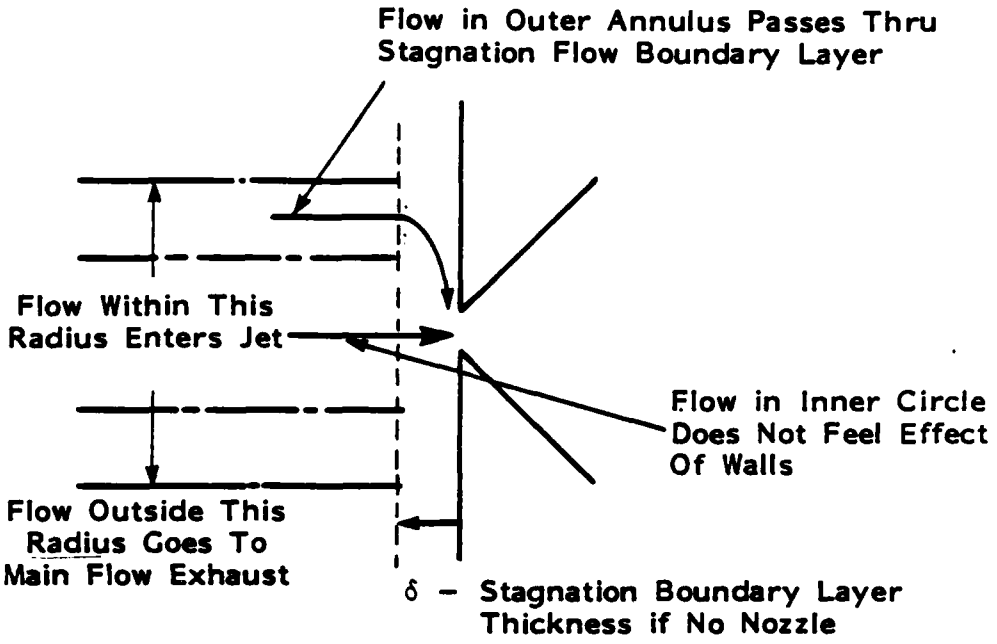

Figure 8a. Assumed Flow Situation When Stagnation Boundary Layer Thickness is Small Relative To the Capture Radius

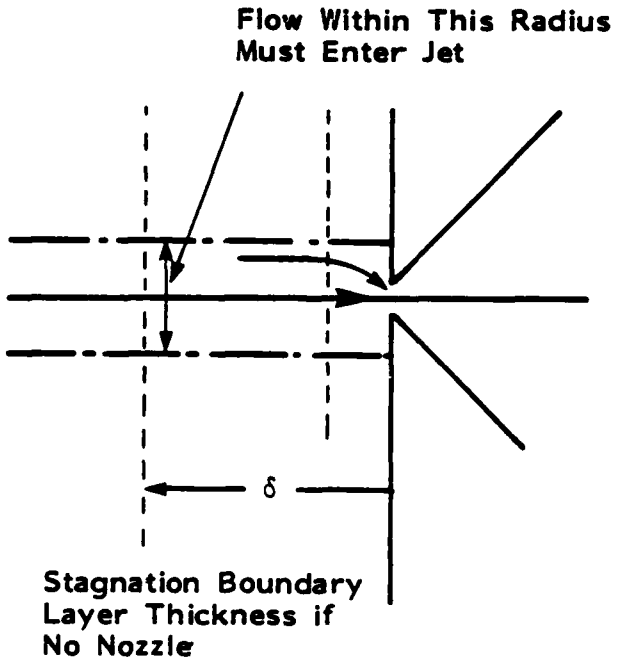

Figure 8b. Assumed Flow Situation When the Stagnation Flow Boundary Layer Thickness is Greater Than the Capture Radius

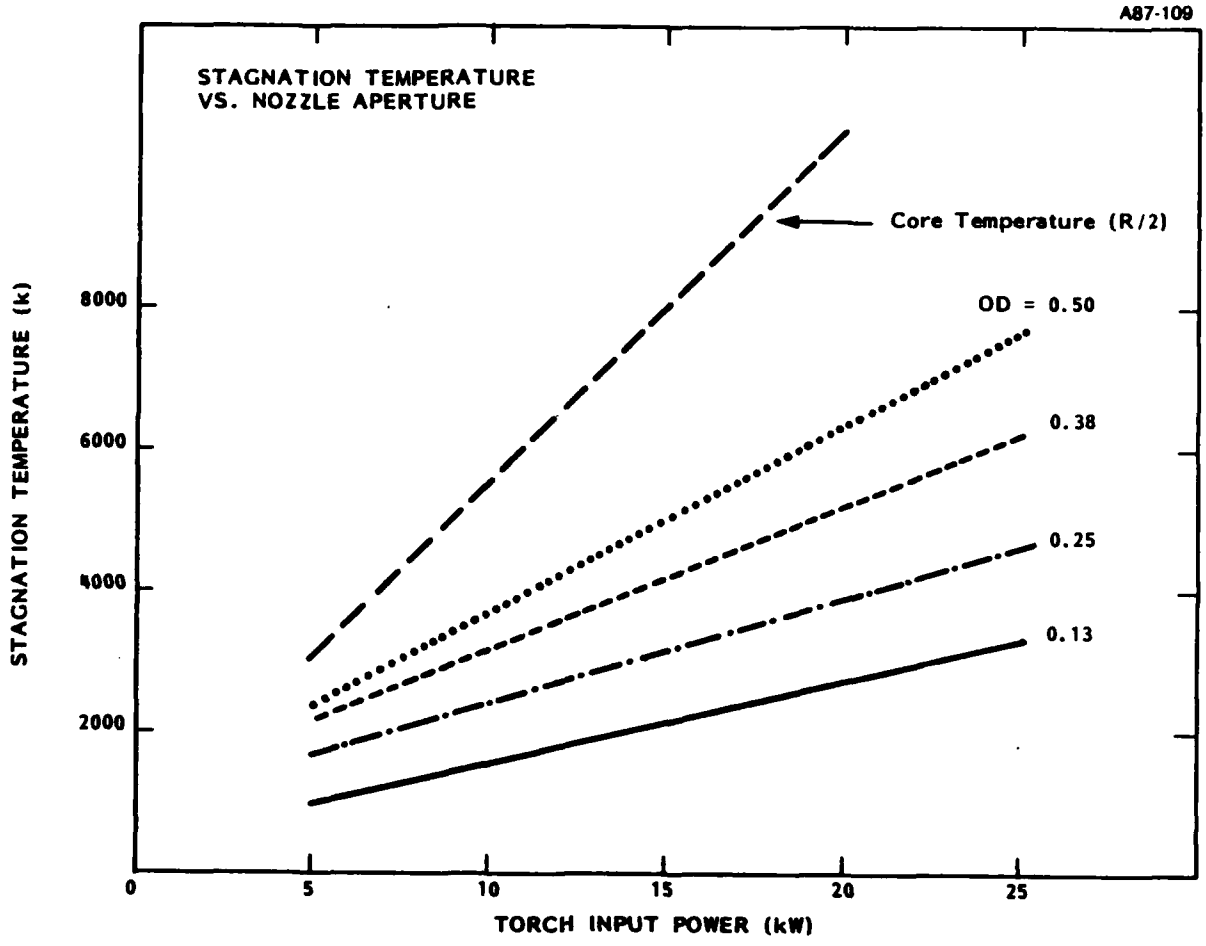

Figure 9. Calculation of Effective Gas Stagnation Temperature Versus Plasma Torch Input Power As a Function of Aperture Diameter. The core gas temperature (R/2) is also noted.

input, with the results shown for two nozzle diameters and two helium flow rates. The influence of nozzle hole size is the result of an increase in capture radius, which reduces the effect of the stagnation wall boundary layer which is fixed in size. The change in nozzle entrance temperature as the helium flow rate changes is small because decreases in boundary layer thickness are offset by decreases in the capture radius.

Losses in the Nozzle and Temperature Profile Leaving the Nozzle

The calculations above do not consider losses in the nozzle itself - the nozzle is designed to have a length to diameter ratio of about 2. On the other hand, the skimmer downstream of the nozzle will be collecting material

from the center of the supersonic jet, which again will be at a higher temperature than the average temperature entering the nozzle.

Comparison with Previous Measurements

In previous measurements the average temperature exiting the nozzle was inferred from the time of flight measurement.[22] For conditions of these experiments (He + 2% oxygen, 110 l min^{-1}, 8 kW, and 5 mil hole) the average temperature of the nozzle gas computed above was 1310 which compares favorably with the measured temperature of 1500. Note that the calculated values underpredict the measured results.

2.2.3 Summary

The average temperature of gas entering the nozzle has been calculated using measured torch/tube heat loss data and a rough fluid flow analysis. The resulting predictions compare favorably with previous measurement of the temperature of the gas exiting the nozzle. The calculations indicate that average temperature in excess of 7000 K can be achieved at torch power levels of 23 kW, a level easily achieved with the torch, mixing tube and nozzle plate designed below. Helium flow rate is not an important parameter so the desirable lower helium flow rate can be used.

2.3 Molecular Beam Modeling

(Note Table 1 presents a list of symbols for the following discussion).

2.3.1 Supersonic Expansion Calculations

The characteristics of any supersonic expansion are properties of the pressure and the temperature of the gas behind the nozzle throat (designated as the stagnation conditions) and the nozzle aperture. For reasons of convenience, most of the useful properties of the expansion are expressed in

Table 1 - Symbol Definitions for Molecular Beam Properties Calculations

Symbols	
M	Mach number
v	flow velocity
c	local speed of sound
γ	ratio of heat capacities C_p/C_v
R	gas constant
T	local temperature
m	molecular weight
X	distance downstream of nozzle
K_{n_o}	Knudsen number
D_o	nozzle diameter
g_o	velocity
n	number density
J	flux (cm^{-2} s^{-1})
F	flow (s^{-1})
P	pressure
S	pumping speed

Subscripts	
0	source or stagnation conditions
1	first vacuum chamber
2	second vacuum chamber
3	third vacuum chamber
T	Terminal
s	skimmer

terms of Mach number M, which is defined as the ratio of the flow speed v to the local speed of sound, c:

$$M = v/c \tag{3}$$

where c is defined as

$$c = (\gamma RT/m)^{1/2} \tag{4}$$

and T is the local gas temperature, γ is the ratio of constant pressure to constant volume heat capacities (C_p/C_v), and m is the molecular weight of the gas. Therefore, one must be able to calculate M at any point downstream in order to know the local number density, temperature, and flow speed. This problem has been solved by method-of-characteristics calculation for the case of an infinitely short nozzle:[28]

$$M(X') = A X'^{\gamma-1} - \frac{\gamma + 1}{2(\gamma - 1)} A^{-1} X'^{1-\gamma} \qquad (5)$$

where

$$X' = \frac{X - X_0}{D_0} \quad . \qquad (6)$$

For $\gamma = 5/3$ (a monatomic gas), A is 3.26, and X_0/D_0 is 0.075 where D_0 is the nozzle diameter, and X is the distance downstream of the nozzle.

In the real world, the Mach number reaches a terminal value, M_T, at which point the number density becomes too low to support further collisions and free molecular flow ensues. As one might expect, this terminal point is a function of the gas itself and the starting conditions in the expansion. Fenn has derived a rigorous expression for this terminal point for a monatomic gas:[29]

$$M_T = 1.17 \; K_{n_o}^{-0.4} \qquad (7)$$

where K_{n_o} is the starting point Knudsen number:

$$K_{n_o} = \lambda/D_0 \qquad (8)$$

and λ is the mean free path at the stagnation temperature and pressure. The local temperature can be expressed in terms of M as:

$$T = T_o \left[1 + \left(\frac{\gamma - 1}{2}\right) M^2 \right]^{-1} \tag{9}$$

and thus the terminal velocity as (remembering that v = Mc):

$$v_T = c_o M_T \left[1t \ \frac{\gamma-1}{2} \ M_T^2 \right]^{-1/2} . \tag{10}$$

In the limit of infinite Mach number, this reduces to:

$$v_T \ (M \to \infty) = \left[\left(\frac{\gamma}{\gamma-1}\right) \ \frac{2RT_0}{m} \right]^{1/2} \tag{11}$$

which demonstrates that for a monatomic gas, a supersonic expansion will produce a beam that is faster than an effusive beam by a factor of 1.58.

In the absence of $M = \infty$, there is a distribution of velocities around the terminal flow velocity given by:

$$f(g) \propto g^3 \exp - \left[(g - v_T)^2 / \alpha^2 \right] \tag{12}$$

where

$$\alpha = \left(\frac{2RT}{m}\right)^{1/2} \tag{13a}$$

$$= \left[\frac{2RT_o}{m} \left(1 + \frac{\gamma-1}{2} M_T^2\right)^{-1} \right]^{1/2} . \tag{13b}$$

Thus, for large M_T, the width of the distribution scales inversely with the Mach number.

The number density as a function of distance from the nozzle throat is given by

$$n = n_o \left(1 + \frac{\gamma-1}{2} M^2\right)^{1/\gamma-1} \quad . \tag{14}$$

Using expression 5 and assuming $M > 4$,

$$M(X) \approx A \left(\frac{X}{D_o}\right)^{\gamma-1}$$

which gives us

$$n(X) = n_o \left[\left(\frac{\gamma-1}{2}\right) A^2\right]^{-1/\gamma-1} \left(\frac{X}{D_o}\right)^{-2} \tag{15}$$

or

$$n(X) = 0.15\ n_o \left(\frac{X}{D_o}\right)^{-2} \tag{16}$$

for a monatomic gas.

The flux, $J(X)$ is just the number density times the flow velocity and at large distances ($X \gg X_T$)

$$J(X) = 0.15\ v_T\ n_o \left(\frac{X}{D_o}\right)^{-2} \quad , \tag{17}$$

When the flux is integrated over all angles, the total flow, F_o, out of the nozzle is

$$F_o = a_o c_o n_o \left(\frac{\gamma+1}{2}\right)^{(\gamma+1)/2(\gamma-1)} . \qquad (18)$$

2.3.2 Zone-of-Silence Calculations

One of the consequences of using a nozzle aperture much larger than in previous studies is an increased gas flow into the vacuum chamber. The chamber used in the studies cited here was pumped by a 32" o.d. diffusion pump with an effective pumping speed of ~16,000 $\ell\ s^{-1}$. Even a pump of this size could not handle the resultant gas flow. We propose to overcome this problem by designing a nozzle-skimmer system based on the work of Roger Campargue.[23-25] This approach is based on the creation of a free-jet zone of silence unaffected by the background gas at relatively high pressure. Optimum performance at this high pressure allows the use of much lower pumping speeds and therefore much physically smaller vacuum systems.

Ideally, experiments would be performed in a zero pressure environment. There would be no interaction between the molecular beam and background gas. These conditions in reality are satisfactorily met when the pressure is maintained below 10^{-3} torr and the beam is separated downstream from the background gas using a skimmer. At these pressures, the beam has reached its full expansion before reaching the skimmer. Unfortunately, given the finite pumping capacity of conventional systems, the throughput of the nozzle is usually limited by either keeping a low source pressure and/or nozzle diameter. If the nozzle is operated at a background pressure of 10^{-2} - 1 torr, the throughput is dramatically increased and/or the required pumping speed reduced. Campargue and co-workers have demonstrated that at these high nozzle pressures, the interaction of the supersonic flow with the ambient background gas produces a well-defined jet shock wave system. The cold core gas of the jet is unaffected by the background gas up to a distance where the

Mach disk of a free jet shock wave structure would be formed in a continuous flow field. This so called "zone of silence" allows the expansion to reach its full extent as if a perfect vacuum existed.

The key to utilizing this effect is to place the skimmer at the proper distance from the nozzle (see Figure 10). Semi-empirically, this distance

$$X_m = 0.125 \left(K_{n_o} P_1 / P_0\right)^{-1/3} \tag{19}$$

where K_{n_o} is the nozzle Knudsen number (the inverse of the mean free path in units of nozzle diameter), P_1 is the background pressure, and P_0 is the nozzle stagnation pressure.

It should be noted that since in this source K and P_0 are fixed at a given source performance, the ability to maintain a reasonable nozzle-skimmer distance is determined by the pumping speed of the vacuum system. We postpone

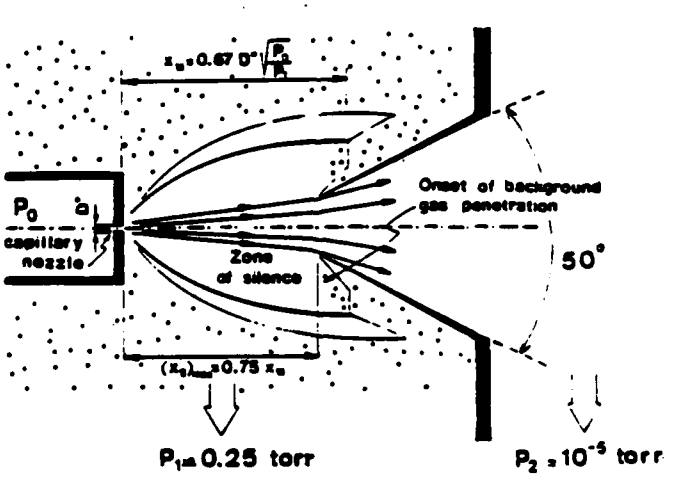

Figure 10. Diagram of a Nozzle Beam Source Operated By Skimming in the Region of Overexpansion of a Free Jet Zone of Silence (taken from Ref. 23)

calculation of this quantity until the discussion of vacuum considerations in theory (Subsection 2.3.3) and in practice (Subsection 3.2). In any case, in order to maintain a standoff of several millimeters, a pressure of less than 0.5 torr must be maintained in chamber 1.

2.3.3 Vacuum Calculations

As noted in the previous section, the performance of the Campargue source depends greatly on the pressure that can be maintained in the first vacuum chamber. This pressure is a function of the nozzle gas flow, F_o and the pumping speed (S_1) in the chamber:

$$P_1 = F_o/S_1 \tag{20}$$

The whole point of the "zone-of-silence" approach is to operate the first chamber in the viscous flow rather than in the molecular flow regime. In this regime, the pumping speed is dependent on the pressure itself.

Let us assume that the pump used has some pumping speed S' at its throat and that the tubing to the chamber has a pumping speed, S'', equal to:[30]

$$S'' = b\,P_1 \tag{21}$$

where

$$b = 2840\ a^4/\ell \quad cm^{-3}\ torr^{-1} \tag{22}$$

when the tube radius a, and length, ℓ, are expressed in centimeters and the pressure in torr. The combined pumping speed of pump and tubing can be expressed as

$$\frac{1}{S} = \frac{1}{S'} + \frac{1}{S''} \quad . \tag{23}$$

Solving Eq. (20) for P_1 leads to:

$$P_1 = \left[\frac{F_o}{S'} + \left(\frac{F_o^2}{S'^2} + \frac{4F_o}{b}\right)^{1/2}\right] /2 \quad . \tag{24}$$

The pressure in the second chamber is dependent on the flow of gas through the skimmer:

$$F_1 = n_s \, v_T \, a_s \tag{25}$$

where

$$n_s = 0.15 \, n_o \left(\frac{X_s}{D_o}\right)^{-2} \quad .$$

Since the skimmer is placed within the "zone-of-silence," by definition it is not sampling any background gas (in any case, flux attributed to background gas in this system is small compared to beam flux). The pressure in chamber 2 is then simply

$$P_2 = F_1/S_2 \tag{26}$$

where S_2 is the pumping speed of the diffusion pump stack in the second chamber.

The pressure in the third chamber is a result of both beam and background contributions to the gas flow:

$$P_3 = F_2/S_3 \qquad - \qquad (27)$$

where

$$F_2 = 0.15\ n_o \left(\frac{X_3}{D_o}\right)^{-2} v_T\ a_3 \qquad (28)$$

$$+ 0.25\ n_2\ \bar{g}_2\ a_3 \quad .$$

In the expression for F_2, a_3 is the area of the aperture into the third chamber, X_3 is the distance downstream of the source of that aperture, n_2 is the number density associated with the background gas in chamber 2, and $\bar{g}_2$ is the average velocity of that gas.

2.4 Source Performance Predictions

2.4.1 Source Properties

Let us assume that we operate the O-atom source at a power rating of 23 kW using a 0.5 mm aperture. According to Figure 9 in Subsection 2.2, the stagnation temperature will be > 7100 K. We will use a gas mixture that is 2% O_2 in helium ($\bar{m}$ = 4.48 g mole^{-1}). The helium collision cross section is 15 A^2 which yields a Knudsen number of 0.01. Using the equations in Subsection 2.3.1, we can now calculate the relevant properties of the molecular beam presented in Table 2. Note that we have considered the gas mixtures as a whole, assuming that there is a negligible velocity slip between the oxygen and helium. In order to calculate the nozzle skimmer distance, we had to make some assumptions about the pressure reached in chamber 1 (~0.065 torr). This will be discussed in Subsection 3.2. Figure 11 presents the expected velocity distribution of the beam at two different torch input powers.

Table 2 - Oxygen Atom Source Operating Conditions

Assumptions	
Torch Input Power (kw)	23
Nozzle Aperture (mm)	0.5
O_2 Content (%)	2.0
Gas Flow (ℓ min^{-1})	60
Results	
Gas Temperature (K)	7100
Mach Number	7.55
Velocity (km s^{-1})	8.0
Flow (torr ℓ s^{-1})	15.5
Nozzle-Skimmer Distance (mm)	7.8

In order to simplify calculations for other operating conditions, Table 3 presents the power dependence of source properties on the operating

Table 3 - Exponential Dependence of Source Properties on Operating Parameters[1]

	T_o	D_o	P_0	P_1
Velocity	0.5	---	---	---
Mach Number	-0.4	0.4	0.4	---
Beam Flux	-0.5	2.0	1.0	---
Nozzle-Skimmer Distance	-0.17	0.67	0.33	-0.33

[1] Constant x B^n where A is a source property (e.g., velocity) and B is an operating parameter (e.g., stagnation temperature, T_o) and n is the exponent listed in the table

parameters. Assume A is a source property such as velocity which depends on source temperature according to the expression

$$A = (\text{constant})\ B^n$$

where the value of n is given in Table 3. Thus the results of Table 2 can be extended to any new set of conditions by:

$$A_2 = A_1 \left(\frac{B_2}{B_1}\right)^n \quad .$$

Figure 11 presents the calculated velocity distributions for two different plasma torch settings. Note that the higher velocity beam also has a larger spread in its distribution. This is the result of a higher Knudsen number at higher temperatures which causes a lower Mach number.

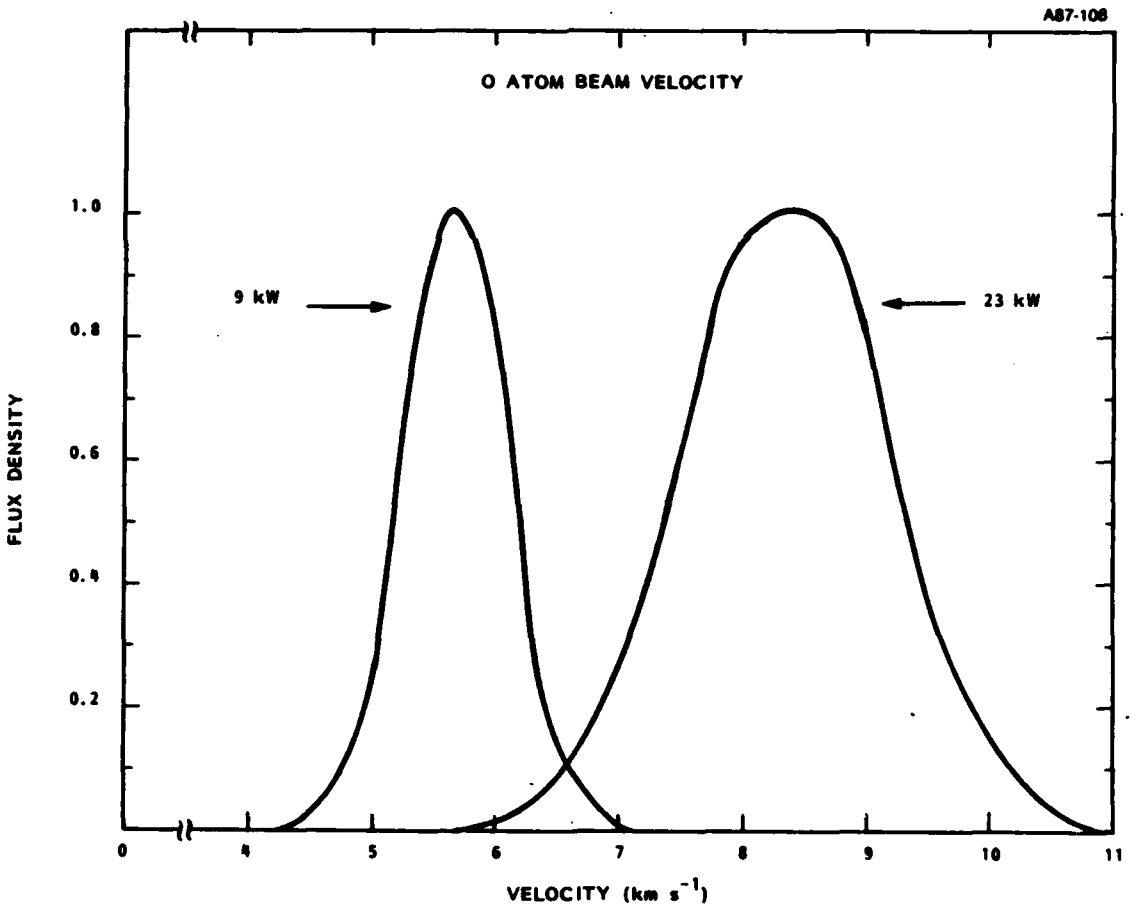

Figure 11. Calculated Velocity Distributions (Flux Density) of Atomic Oxygen In Helium Carrier Gas At Two Different Plasma Torch Input Powers

2.4.2 Metastable Population

One problem of any high temperature source is the presence of metastable species in the beam. In this case, atomic oxygen has two comparatively low-lying states, ^1D at 1.967 eV and ^1S at 4.189 eV. In addition, He itself has its first excited state ^1P at 21.217 eV. It should be stressed that any metastable population should be equal to that predicted by equilibrium calculations in this source because of the fact that it is operated at a stagnation pressure of one atmosphere. In addition, the oxygen is admixed into the main flow downstream of the discharge itself, thus precluding the production of a suprathermal concentration of metastable or ionic species. It should be emphasized that seeding the oxygen in the much lighter helium carrier gas allows us to reach high velocities at a much lower temperature than would be required in the case of a pure oxygen flow. The latter case would require a source temperature of 28000 K, producing much higher metastable species concentration.

The fraction of molecules in an excited state can be approximately determined by

$$\frac{n^*}{n} = \frac{g^*}{g} \exp[-(E_o/RT)] \tag{29}$$

where * denotes the excited species, g is the degeneracy and E_o is the term energy for that state. Table 4 presents the relative populations of various, oxygen, and helium states in the beam assuming a 2% mixture of O_2 in helium and a stagnation temperature of 7100 K. One should note that at most metastable species represent 0.1% of the total beam.

We now address the question of whether the metastable species are quenched upon entering the supersonic expansion. While it is true that the effective local temperature of the expanded gas becomes quite small (~350 K is this case), the effective interaction time may be too short to allow much

Table 4 - Relative Population of Various Species in the Molecular Beam (T = 7100 K)

Species	g	E_o (eV)	Percent (%)
O (^{3}P)	9	0	3.9
O (^{1}D)	5	1.967	8.4×10^{-2}
O (^{1}S)	1	4.184	4.8×10^{-4}
He (^{1}S)	1	0	96
He (^{1}P)	3	21.217	2.5×10^{-13}

quenching. For example, the quenching rate of a species A* can be represented as:

$$-\frac{d\,A^*}{dt} = k_Q\,A^*B \qquad (30)$$

where k_Q is the quenching rate constant and B is the concentration of all species. Since B is constantly changing as a function of distance downstream of the nozzle, it it is convenient to note that

$$B = n_o\,(T/T_o)^{1/\gamma-1}$$

where

$$\frac{T}{T_o} = \left(1 + \frac{\gamma-1}{2}\,M^2\right)^{-1} .$$

Given that

$$-\frac{d\,A^*}{dT} = -\frac{dA}{dX}\,\frac{dX}{dT} \qquad (31)$$

we arrive at:

$$\frac{d A^*}{dX} = \frac{K A^* B}{v} \tag{32}$$

where the flow velocity, v is just

$$v = M c_0 \left(1 + \frac{\gamma - 1}{2} M^2 \right)^{-1/2} \tag{33}$$

Rearranging Eq. (31) and expressing it in terms of Mach number, M, we arrive at

$$\frac{d A^*}{A^*} = \frac{K_Q B_0}{c_0} \left[M \left(1 + \frac{M^2}{3} \right) \right]^{-1} dX \quad . \tag{34}$$

Integrating this expression, we obtain

$$\frac{A_T^*}{A_0^*} = \exp - \int_0^{X_T} \frac{K_Q B_o D_o}{c_o} \left(M + \frac{M^3}{3} \right)^{-1} d\left(\frac{X}{D_o}\right) \tag{35}$$

where the expression is integrated from X=0 to X_T, the terminal expansion distance. This expression can be evaluated if M is fully known as a function of X. Unfortunately, M has been solved only from $X/D_0 = 1$; the solution presented in Subsection 2.3.1 cannot accurately predict M for values less than that. In this case, we have extrapolated the results to X=0 (knowing that M=1 at X=0 by definition) and roughly integrated the above expression to give

$$\ln \frac{A^*}{A_0^*} \approx - \frac{K_Q B_o D_o}{3 c_o} \tag{36}$$

in the limit that the quenching rate constant is not a strong function of temperature (not necessarily a good assumption!).

In our case (T=7100 K, D_o=0.5 cm, m=4.48 g mole^{-1}),

$$\ln \frac{A^*}{A^*_o} \approx - 3.7 \times 10^{10} K_Q \quad . \tag{37}$$

Thus, if the quenching rate constant is gas kinetic ~ 2×10^{-10} cm^3 s^{-1}, [as one might expect for O(^{1}D)]

$$\frac{A^*_T}{A^*_0} \approx 10^{-3} \quad .$$

If, on the other hand, quenching is inefficient (K_Q ~10^{-14} cm^3 s^{-1}) as it is for O(^{1}S),

$$\frac{A^*_T}{A^*_o} \approx 1.0 \quad .$$

The point of this exercise is to show that for species which are <u>efficiently</u> quenched, such s O(^{2}D), the nozzle expansion <u>may</u> be efficient at reducing the metastable population. If the species is <u>not efficiently</u> quenched the expansion <u>will not</u> reduce their concentration.

In summary, we estimate that the major electronically excited species in the beam will be O(^{1}D) at concentrations between 10^{-2} and 10^{-4} of ground state O(^{3}P). These metastable levels are sufficiently low to insure that materials studies will be dominated by interactions with ground state atomic oxygen.

(It should be noted that the ambient sunlit space environment contains non-negligible quantities of metastable oxygen atoms. At 200 kilometers altitude, Torr and Torr predict fractional concentrations [compared to $O(^3P)$] of $O(^1D)$ and $O(^1S)$ of 10^{-4} and 10^{-7} respectively for a noontime thermospheric model.[31] Furthermore, these ratios increase significantly at higher altitudes.

3.0 APPARATUS

This section is divided into three parts describing the beam source, the vacuum system, and the detection system. The first two contain fairly detailed schematic diagrams of the apparatus as it is currently envisioned. We note that in order to obtain accurate cost estimates, planning of these parts has exceeded the level of detail shown in the figures. The last part contains calculations necessary to ascertain the level of system performance.

3.1 Oxygen Atom Beam Source

As noted previously, we have opted to build the beam source in a modular fashion so as to optimize the flexibility of the source design. While initial costs are slightly higher as compared to an integral source, subsequent modifications will be much cheaper and faster. A cutaway assembly view is presented in Figure 12. Aside from the plasma torch itself, (Model 91, Tafa Corporation), the source will be comprised of four parts (all constructed from OFHC copper using electron beam welding): the injector, two or more spacers, an exhaust section, and a nozzle plate. All the components can be bolted together and eventually to the apparatus front flange with an O-ring seal. In order to provide sufficient cooling capacity, a high pressure water pump will be used to provide a several gallon per minute water flow at 300 psi pressure.

Oxygen will be admixed into the heated gas flow from the plasma torch in the injector section. As shown in Figure 13, the injector will contain four injector ports, each with a 0.25 mm aperture, connected to a common oxygen inlet port. Each individual port can be blocked by inserting a nylon screw. The port itself will be pointed slightly upstream so as to facilitate mixing and provide machining clearance. The distance over which the oxygen and main gas flow mix will be controlled by inserting spacer parts (shown in Figure 14). Each spacer will be approximately 3/8" long and will be inserted as necessary to optimize source performance.

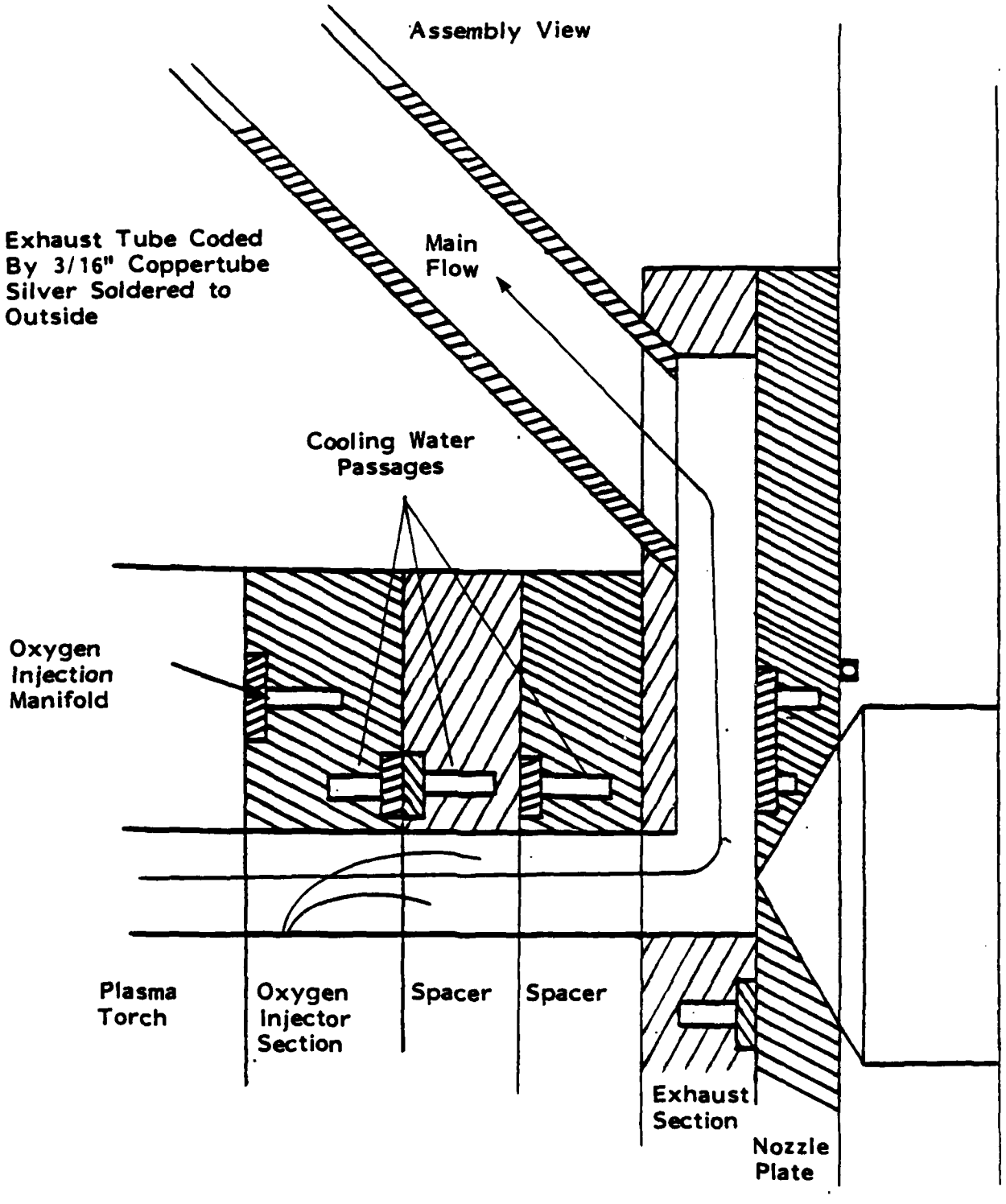

Figure 12. Schematic Showing Cutaway Assembly View

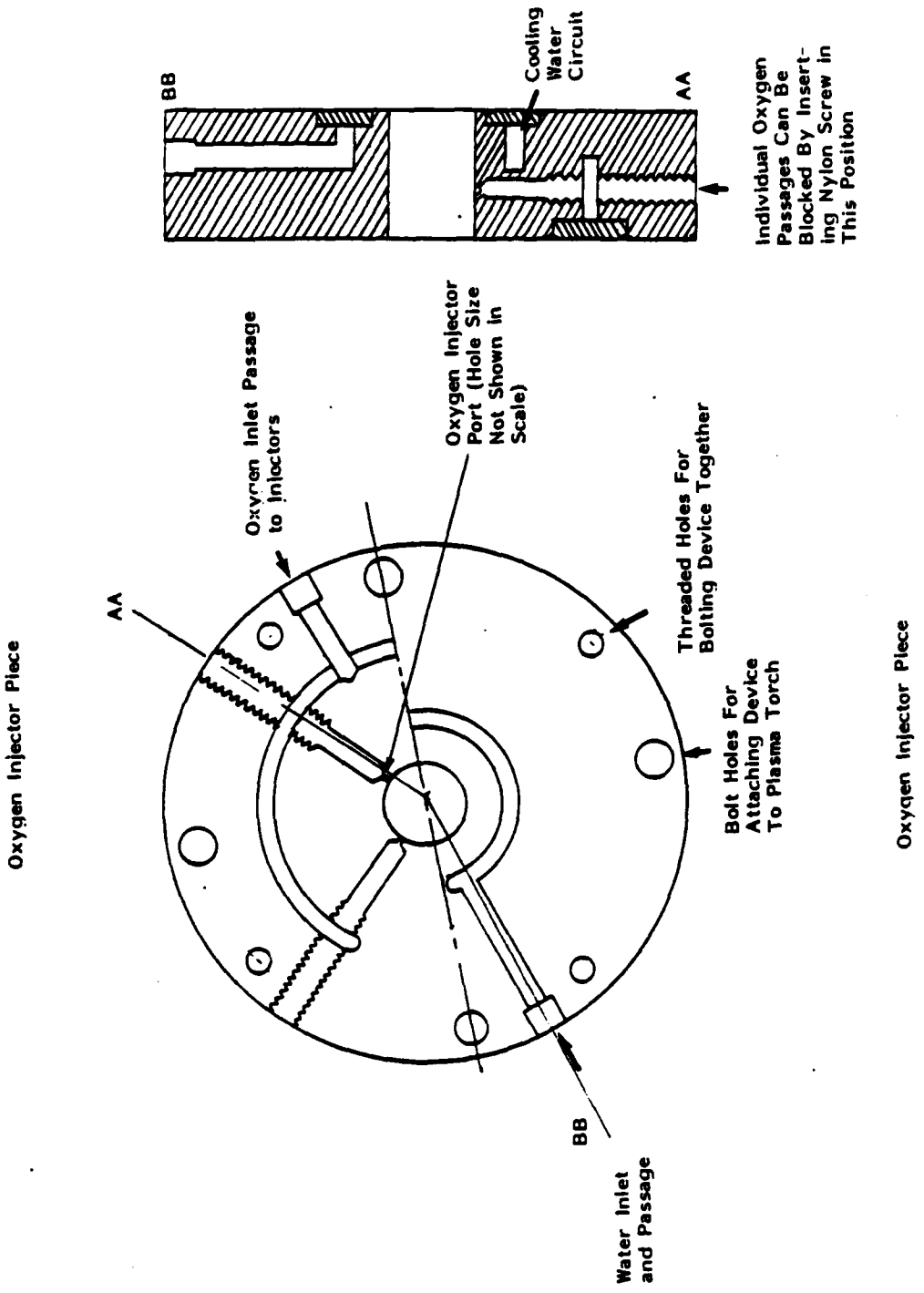

Figure 13. Oxygen Injector Piece

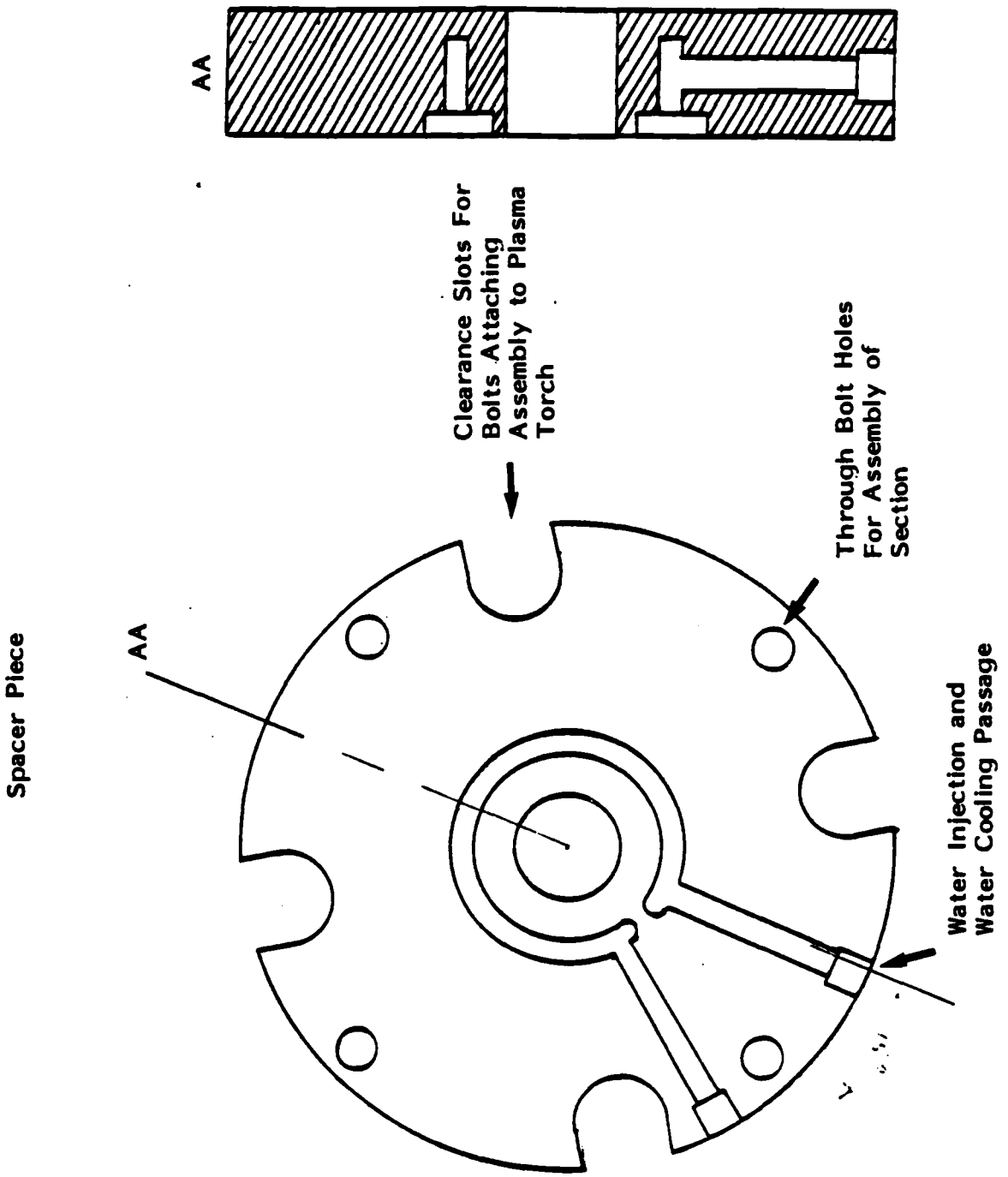

Figure 14. Spacer Piece

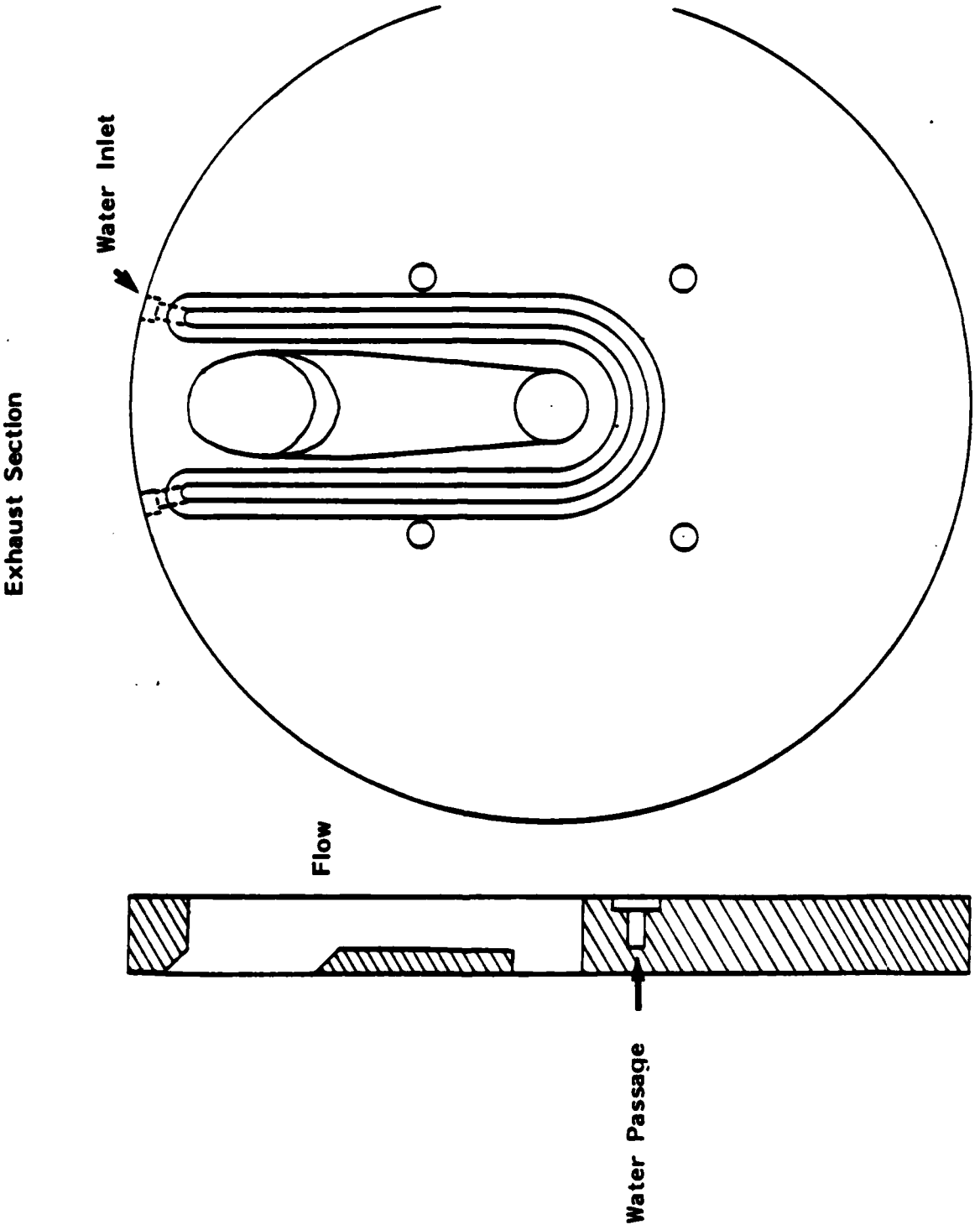

Figure 15. Exhaust Section. Note that the water passage surrounds the flow passage.

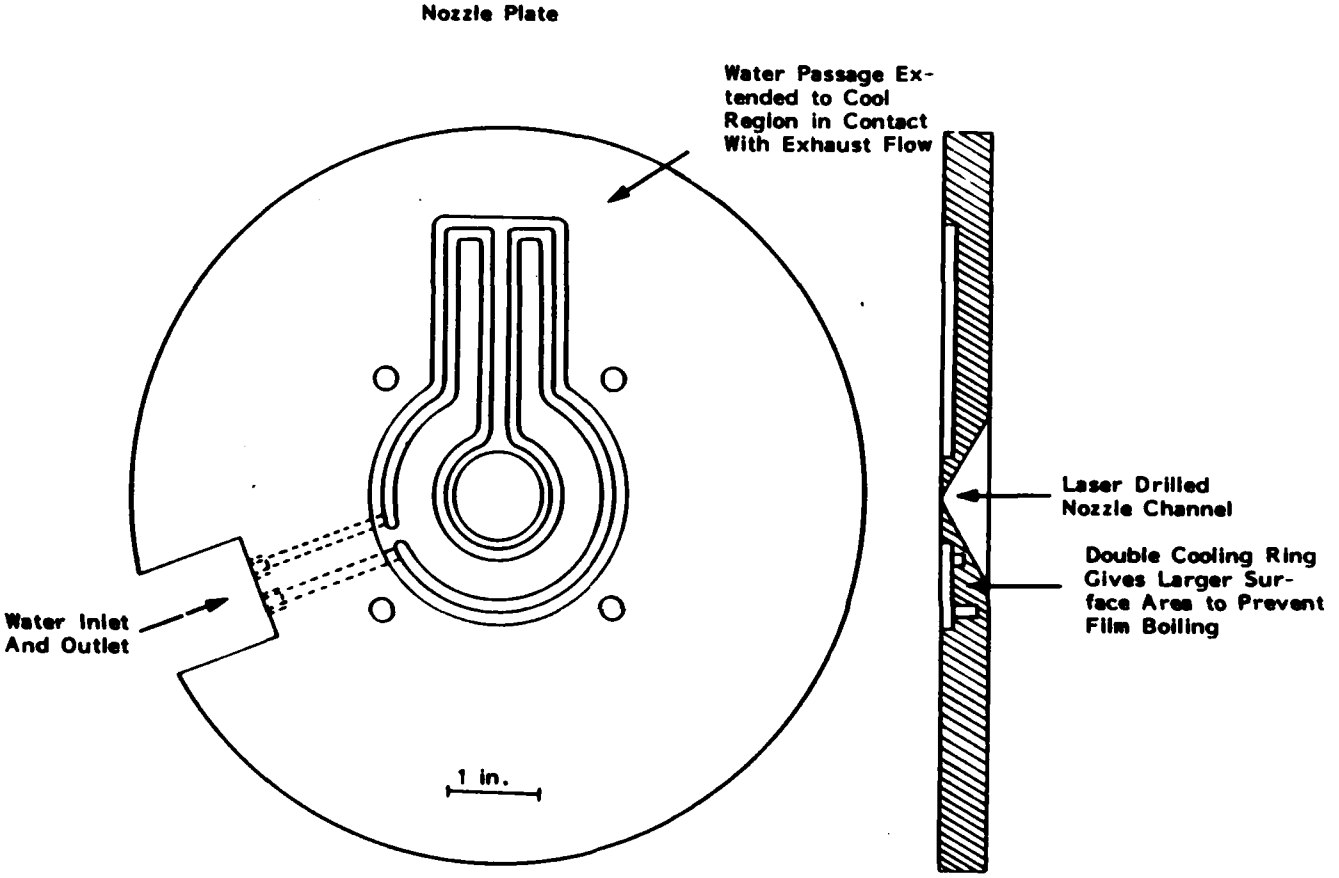

Figure 16. Nozzle Plate

At this point, the gas mixture will flow into the exhaust section and strike the nozzle plate. Most of the gas flow will continue off to one side and into the exhaust port where it will be vented into a hood. A small fraction (10^{-3}) will expand through the nozzle aperture to form the exhaust section and nozzle plate respectively. The heat load on these parts is substantial and the design reflects the need to bring water cooling as close to the gas flow passages as possible. These designs are a refinement of our previous effort which was quite successful in relieving the heat stress. The final nozzle aperture will be drilled using a laser. This technique will easily provide 40 μm accuracy.

3.2 Vacuum System

A schematic of the vacuum apparatus is presented in Figure 17. It is comprised of three cylindrical chambers, all constructed of stainless steel. The schematic is drawn to scale assuming that the apparatus diameter is ten inches. Each chamber is to be constructed with a large access port and additional instrumentation and view ports. We have chosen to use Con-flat mating flanges wherever possible as they are compact, comparatively inexpensive, and easily obtainable. In the third chamber, where ultra-high vacuum is desired and in the main flange interfaces, copper gaskets will be used; for often used ports, Viton o-rings or Viton gaskets will suffice.

The first chamber, approximately six inches long, has a 4" o.d. outlet to the pumping system. This outlet is connected to a Roots blower (pumping speed ~700 $\ell\ s^{-1}$) through approximately 150 cm of 7.5 cm i.d. and 900 cm of 15 cm i.d. tubing. The effective pumping speed of the tubing can be expressed as (using Equations 21 and 22 in Section 2.3.3):

$$S'' = 5500\ \Delta P \quad .$$

yielding [using Eq. (24)] a pressure rise of 0.065 torr in the first chamber when the oxygen atom source is being utilized. Using Eq. (19) in Subsection 2.3.2, we find that the skimmer distance should be held at 6.3 mm for

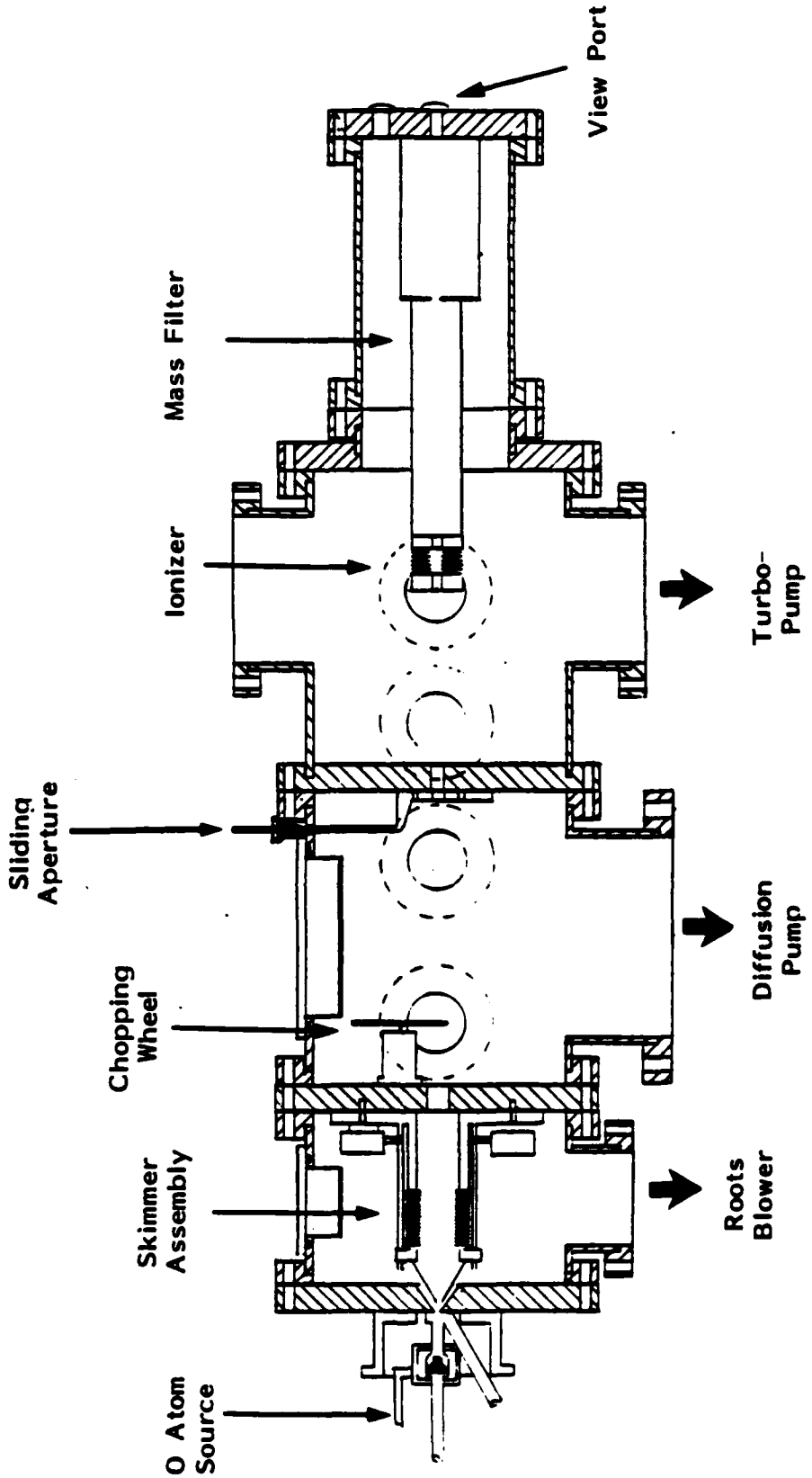

Figure 17. Schematic of Atomic Oxygen Molecular Beam Apparatus

best source performance. The skimmer is mounted on a bellows assembly which will be equipped with remote x-y-z translation capabilities so as to optimize positioning.

The second chamber, approximately 10" long, will house the beam chopper as well as provide access ports for laser beams, radiometers, microbalances, etc. for future studies. It will be pumped by a 6" diffusion pump which provides the most cost effective pumping. In this case, it will suffice as an extremely clean system which is not needed for this experiment. In the future, though, if hydrocarbon contamination is a problem, a turbomolecular pump can be used.

The third chamber is an ultrahigh vacuum chamber which houses the quadrupole mass spectrometer. It is configured so that the mass filter can lie on the beam axis or orthogonal to it. The latter arrangement, although offering less sensitive detection, avoids the possible problem of light from the arc source ionizing molecules past the ionizer; this can interfere in measuring time-of-flight spectra. In order to maintain a pressure below 10^{-7} torr while the beam is entering the third chamber, a 1000 $\ell\ s^{-1}$ turbomolecular pump is attached. The compression ratio of this type of pump for helium is poor (10^4) and a second, much smaller turbopump must be utilized as an intermediate stage before the roughing pump.

Table 5 presents a summary of chamber apertures, distances, and effective pumping speeds for the proposed apparatus. The flows attributable to the beam itself and the ambient background are calculated according to the equations in Subsection 2.3.3. It should be noted that if the "zone-of-silence" principle is operative, there is no background gas leaking into the second chamber.

A notable feature of the design is the ability to align the nozzle-skimmer system with the detector under vacuum. We will purchase the mass filter with a viewport that will allow a line of sight through the ionizer and subsequent apertures. Both the nozzle assembly and third chamber apertures will be adjustable under vacuum. Final adjustments will be made by maximizing the intensity of the oxygen atom signal.

Table 5 - Calculated Vacuum Chamber Operating Conditions

Po = 760 Torr, To - 7100 K	Chamber 1	Chamber 2	Chamber 3
Aperture Area (cm^2)	0.002	0.002	0.002
Aperture Distance (cm)	0	0.65	45
Beam Flow (torr ℓ s^{-1})	15.5	0.044	8×10^{-6}
Background Flow (torr ℓ s^{-1})	----	----	8×10^{-6}
Pumping Speed (ℓ s^{-1})	240	1000	1000
Background Pressure (Torr)	6.5×10^{-2}	4×10^{-5}	2×10^{-8}

3.3 Detection System

The identity of the species in the beam will be identified using an Extrel quadrupole mass spectrometer system comprised of an electron bombardment ionizer, quadrupole mass filter, and Channeltron particle multiplier. The detector axis will be orthogonal to the beam axis so as to minimize contributions to the signal from photoionization due to light from the source or from surface-metastable collisions. Measurement of the fractional dissociation of molecular oxygen as well as beam velocity will be carried out as explained in Reference 22.

Calculation of the expected signal can be performed in the following manner. The entrance aperture to Chamber 3 has been chosen so that the entire flow attributable to the beam which enters the third chamber (F_3') will enter the ionizer. The signal attributable to the beam itself can be calculated as:

$$S_{Beam} = E_i F_3' \chi_o \tag{38}$$

where E_i is the overall detector efficiency (10^{-4} -10^{-8}) and χ_o is the Oxygen atom mole fraction (0.04). Since the beam flow into Chamber 3 is 6.7×10^{14} s^{-1} (see Table 5), the calculated signal is:

$$S \text{ (oxygen)} = 1.2 \times 10^{7} \text{ } s^{-1} \qquad (E_i \approx 10^{-6}) \tag{39}$$

or if the multiplier has a gain of 10^6 and a 10^6 ohm input resistor is used, a 2 volt(!) signal is generated.

One source of background is attributable to background gas from Chamber 2 which effuses into Chamber 3 and strikes the ionizer. In the effusive limit,

$$F_{background} = \frac{\chi_o n_2}{4} \bar{g} \frac{A_3 A_d}{L^2} \tag{40}$$

where n_2 is the Chamber 2 number density, A_3 is the area of the aperture into Chamber 3, A_d is the area of the ionizer opening, and L is the distance from the chamber aperture to the ionizer. The mole fraction of oxygen atoms (χ_o) will necessarily be much lower than in the beam but since molecular oxygen will fragment in the ionizer, we can assume the same value as in the beam as an upper limit. Consulting Table 5 and assigning L=30 cm and $A_d = 0.2$ cm^2, and noting that

$$\bar{g} = \left(\frac{8RT}{\pi M}\right)^{1/2} \tag{41}$$

we find that

$$F_{background} = 3.1 \times 10^{8} \quad .$$

This results in a signal of

$$S_{background} < 310 \quad .$$

or 10^{-5} of the signal from the beam.

One other contribution to the noise is the signal due to the background in the third chamber. Based on information from Extrel, we can assign an ionization efficiency of 6×10^{16} ions $torr^{-1}$ background gas. Again consulting Table 5, we obtain a signal of

$$S'_{background} < 1.5 \times 10^{5}$$

which is 200 times lower than the beam signal.

Absolute calibration of the beam flux will be accomplished using an ion gauge measurement technique developed in the laboratories of Herschbach and Lee (D. Worsnop, Private Communication). An ion gauge tube with only one opening is placed in the path of the beam. The pressure in the tube rises above ambient until the flow into the tube matches the flow out of the tube:

$$F_{beam} = P_{tube} S_{tube}$$

where the pumping speed of the tube aperture, S_{tube}, can be calculated using the tables in Ref. 30. Therefore, the beam flux is linearly proportional to the measured pressure rise. The expected pressure rise at 30 cm downstream of the source is calculated to be approximately 10^{-5} torr, an easily measured

quantity. This exceedingly simple technique is not sensitive to the high beam energy as the gas is thermally accommodated in the tube. Calibration of the mass spectrometer is exceedingly difficult due to the fact that the spectrometer sensitivity is a function of the incoming beam energy. Compargue (Private Communication) has pointed out that using a room temperature effusive beam for calibration may not accurately reflect the spectrometer performance at high beam energies. Specifically, the efficiency of ion collection system used to focus the ions out of the ionizer drops as the neutral beam energy starts to approach the ion energy used in the Extrel system (typically 20 eV).

In summary, we conclude that the properties of the beam can be measured with very large signal-to-noise ratios.

4. CONCLUSIONS

4.1 Phase I Summary

Production of a supersonic beam of atomic oxygen by electric discharge heating appears to be an optimum approach to the problem. The results of our modeling indicate that all the design goals can be met. Table 6 presents our best estimates of the source temperature and dissociation efficiency, as well as the beam velocity and flux. Note that the last quantity is quoted at a given distance (10 cm) from the source so that the flux at a reasonable working distance can be calculated (knowing that flux is inversely proportional to the square of the distance).

A great advantage of this approach is the flexibility allowed in the performance characteristics of the source. Simply by dialing in the input power to the plasma torch, the velocity can be varied from 5-8 kms^{-1} and with the use of argon as a carrier gas, the lower limit can be reduced to ~2 kms^{-1}, or an energy range of 0.3 - 5.0 eV. One can also vary the oxygen atom flux to any desired degree by diluting its flow through the injector without changing any of the other operating parameters. Thus one can study isolated gas-surface interactions at low fluxes (10^{12} cm^{-2} s^{-1}) and surface chemistry at high fluxes (10^{16} cm^{-2} s^{-1}). In terms of simulating Low Earth Orbit, the flux at 30 cm is approximately 100 times that at an altitude of 300 km. The newly instituted NASA-sponsored Atomic Oxygen Effects Test Program calls for a

Table 6 - Beam Source Predictions

	Old Source	New Source
Temperature (K)	1500	7100
Velocity (km s^{-1})	3.8	8.0
Dissociation Efficiency (%)	30	100
Flux at 10 cm (cm^{-2} s^{-1})	1 x 10^{16}	1 x 10^{17}

total exposure of 3.5×10^{20} atoms cm^{-2}. This can be attained in only ten hours of exposure time!

We have designed both the source and the vacuum system to be completely modular so that rapid and comparatively inexpensive changes can be made. The source is divided into four parts (plasma torch, injector, mixing tube, and end plate), all of which can be redesigned and replaced at will. The vacuum chamber is divided into three separate chambers, all of them containing extra ports for the possible inclusion of new instrumentation. It would not be unreasonable to have several extra chambers specifically designed for particular experiments.

4.2 Future Work

We propose that a Phase II project concentrate on the final design, construction and testing of the atomic oxygen beam source. If time permits, simple erosion tests can be performed to prove the efficacy of the source. We expect the performance of this task to take the two years duration of a possible Phase II project. At this point, a program utilizing the source can proceed in several different directions. Several possibilities are discussed below.

Gas Phase Interactions

The ability to generate very fast beams of light atoms opens up new avenues of research for crossed beams chemistry. The fundamental reactivity of oxygen and nitrogen atoms (at conditions producing 8 km s^{-1} beams, nitrogen is totally dissociated into atoms) at high energies have not been extensively studied under single collision conditions. The most popular technique for studying "hot atom chemistry" today involves photodissociating precursor molecules to produce fast moving atoms which the collide with an ambient gas bath (see Ref. 32). While producing many interesting results, the technique is not "tunable" with respect to energy for any given atom; indeed it is

non-trivial to find a precursor molecule which would produce O or N atoms exclusively in their ground states at an accessible wavelength. Thus the ability to use molecular beams would complement these studies.

From a standpoint of fundamental concern to gas phase chemical dynamics, the following chemical reactions would be of great interest:

$$O + H_2 \rightarrow OH + H$$
$$O + H_2O \rightarrow OH + OH$$
$$N + H_2O \rightarrow OH + NH$$
$$N + O_2 \rightarrow NO + O$$
$$O + CH_4 \rightarrow OH + CH_3$$

where the vibrational excitation of the product diatomic molecule(s) could be probed using laser induced fluorescence. The first, of course, is a basis for combustion in hydrogen flames and a prototype for hydrocarbon combustion. Calculations by Schinke and Lester[33] indicate a reaction threshold of approximately 0.45 eV. The relative translational energy attainable with this source is approximately 1 eV; study of this threshold region would be an excellent test of theory, both in confirming threshold energy calculations as well as the energy dependence of the reaction cross section. Similar arguments hold for the reactions of nitrogen atoms, whose high velocity behavior has been virtually ignored except for the work of Bernstein's group[34] whose source, unfortunately, was contaminated with large amounts of metastable atoms.

Another class of chemical interactions whose behavior is poorly understood is that of collisional vibrational excitation. For example:

$$O + H_2O \rightarrow O + H_2O^{\neq}$$
$$O + CO_2 \rightarrow O + CO_2^{\neq}$$
$$O + CO \rightarrow O + CO^{\neq}$$
$$O + HF \rightarrow O + HF^{\neq}$$
$$O + HCl \rightarrow O + HCl^{\neq}$$

where $\neq$ denotes vibrational excitation are all of great interest to the rocket exhaust plume signature community. Indeed, the original motive for the development of this atomic oxygen source was to study the first two processes shown above. At the relative energies attainable with the old version of the source (0.6 eV), the apparent cross sections for excitation of the ν_3 modes were below the detectable limit (0.05 A^2). Calculations by Redmon, Schatz, and Garret[35] indicate that for H_2O, the cross section at 0.6 eV was only 0.01 A^2, in accord with the null result. But at the newly attainable relative collision energy of 2.7 eV, the cross section should rise to several tenths of a square A^2. Similar calculations indicate that CO, HF, and HCl should behave in a like manner. Just being able to measure the relative excitation cross sections as a function of incident collision energy to compare with theory would be extremely useful for the modeling of rocket plume signatures.

Gas Surface Interactions

From a practical point of view, one of the highest priority uses for an oxygen atom source is to test space-based materials for their erosion properties. Anticipated erosion of materials facing the atmospheric wind would threaten the integrity and/or performance capability of many structures. The simplest evaluations would involve making weight loss measurements using a quartz crystal microbalance. A further enhancement of these studies would include mass spectrometric analysis of the resultant gas phase products, which allow identification of the reaction pathways. Use of time-of-flight measurement techniques producing information on the translational energy of these products coupled with induced-fluorescence probing of their internal excitation would answer the question of whether the

surface reaction chemistry was "impulsive" or governed by thermal accommodation with the surface. If the latter holds, the surface chemistry might be quite varied and complicated.

A related subject in the problem of materials degradation concerns the material left on the surface after erosion has taken place. For instance, thin metal films may totally erode or passivate depending on whether they form volatile or stable oxides.[36] Electrical properties may change from conductive to insulating, and optical transmission characteristics may be completely altered. In the case of lubricated sliding surfaces, tribological properties might be drastically altered. In these circumstances, in-situ surface analysis techniques such as x-ray photoelectron (XPS), Auger, and surface Raman, and low energy electron loss spectroscopy would be useful tools.

An example of the types of surface chemistry which can occur can be obtained from the literature on etching of silicon by fluorine compounds. It was initially thought that only a monolayer of fluorinated silicon was formed in reactions with fluorine atoms.[37] Using x-ray photoelectron spectroscopy and an atomic fluorine beam source, we were able to demonstrate that fluorine atoms penetrated and reacted with the lattice to a depth of at least 10 monolayers and that as fluorine atom uptake increased, the fluorinated surface layer evolved to include SiF_2-like, SiF_3-like and SiF_4-like species.[38] Similar behavior might be expected for atomic nitrogen and oxygen. Studies in this area would be of great concern to the semiconductor materials community; the ability to controllably grow silicon oxynitride (Si-N-O) from silicon or silica using nitrogen and oxygen atom bombardment would be of particular interest since its insulating properties are superior to silica in some respects.

A nascent area of research involves the photostimulated surface chemistry. This may be extremely important in space due to the large ultraviolet solar flux. Recent results indicate for instance, that silicon dioxide, normally quite inert to further reaction, can be made unstable by

excimer radiation at 193 or 248 nm. It is thought that the UV photon may have an effect similar to ion bombardment. These results suggest that the costimulus of high energy atom bombardment and UV photon irradiation may have completely unforeseen effects on materials.

In conclusion, the development of a high (and tunable) energy, supersonic atomic beam source will be a useful tool in several areas of study which are useful to the space contamination, semiconductor materials, rocket plume, atmospheric sciences, and chemical physics communities.

5. REFERENCES

1. L.J. Leger, "Oxygen Atom Reaction With Shuttle Materials at Orbital Altitudes," NASA Technical Memorandum 58246 (May 1982).

2. L.J. Leger, J.J. Visentine, and J.F. Kuminecz, "Low Earth Orbit Atomic Oxygen Effects on Surfaces," AIAA Paper 84-0548 (January 1984).

3. A. Whitaker, "LEO Effects on Spacecraft Materials," AIAA Paper 83-2632-CP (November 1983).

4. P. Fraundorf, D. Lindstrom, N. Pailer, S. Sanford, P. Swan, R. Walker, and E. Zinner, "Erosion of Mylar and Protection by Thin Metal Films," AIAA Paper 83-2636 (November 1983).

5. J.J. Park, T.R. Gull, H. Herzig, and A.R. Toft, "Effects of Atomic Oxygen on Paint and Optical Coatings," AIAA Paper 83-2635CP (November 1983).

6. P.N. Peterson, R.C. Linton, and E.R. Miller, Geophys. Res. Lett. 10, 564 (1983).

7. J.H. Yee and V.J. Abreu, ibid, 10, 126 (1983).

8. M.R. Torr, ibid 10, 114 (1983).

9. P.M. Banks, P.R. Williamson, and W.J. Raitt, ibid, 10, 118 (1983).

10. S.B. Mende, O.K. Garriott, and P.M. Banks, ibid, 10, 122 (1983).

11. J.H. Yee, V.J. Abreu, and A. Dalgarno, ibid, 11, 192 (1984).

12. S.B. Mende, R. Nobles, P.M. Banks, O.K. Garriott, and J. Hoffman, J. Spacecraft 21, 374 (1984).

13. L.J. Leger and J.T. Visentine, J. Spacecraft 23, 505 (1986).

14. G.S. Arnold, D.R. Peplinski and F.M. Carascano, Space Division Report SD-TR-86-58 (September 1986).

15. J. Geddes, P.N. Clough, and P.L. Moore, J. Chem. Phys. 61, 2145 (1974).

16. S.J. Sibener, R.J. Buss, C.Y. Ng, and Y.T. Lee, Rev. Sci. Instrum. 51, 167 (1980).

17. D.R. Miller and D.F. Patch, Rev. Sci. Instrum. 40, 1566 (1969).

18. R.J. Buss, P. Casavecchia, T. Hirooka, S.J. Sibener, and Y.T. Lee, Chem. Phys. Lett. 82, 396 (1981).

19. P.A. Gorry, C.V. Nowikow, and R. Grice, Chem. Phys. Lett. 49, 116 (1977).

20. D.H. Winicur and E.L. Knuth, J. Chem. Phys. 46, 4318 (1967); W.S. Young, W.E. Rodgers, and E.L. Knuth, Rev. Sci. Instrum. 40, 1346 (1969); W.S. Yong and E.L. Knuth, Entropie 30, 25 (1969); D.H. Winicur, E.L. Knuth, and W.E. Rodgers, Entropie 30, 154 (1969).

21. R.W. Bickes, K.R. Newton, J.M. Herrmann, and R.B. Bernstein, J. Chem. Phys. 64, 3648 (1976).

22. J. Silver, A. Freedman, C.E. Kolb, A. Rahbee, and C.P. Dolan, Rev. Sci. Instrum. 53, 1714 (1982).

23. R. Campargue, J. Phys. Chem. 88, 4466 (1984).

24. R. Campargue, A. Lebehot, J.C. Lemonnier, and D. Marrette, "Rarified Gas Dynamics," 12th Symposium, Vol II, S.S. Fisher, Ed., AIAA, New York (1981).

25. R. Campargue, A. Lebehot, and J.C. Lemonnier, "Rarified Gas Dynamics," 10th Symposium, Vol, II, J. Leith Potter, Ed., AIAA, New York (1977).

26. Abramovich, G.N., "The Theory of Turbulent Jets," MIT Press, Cambridge, MA (1963).

27. Schlichting, H., "Boundary Layer Theory," McGraw Hill, New York (1968).

28. H. Ashkenas and F.S. Sherman, Advances in Applied Mechanics, Supplement 3, Rarified Gas Dynamics (1965), J.H. de Leeuwied Vol II, p.84.

29. J. Anderson and J. Fenn, Physics of Fluids, 8, 780 (1965).

30. S. Dushman, Vacuum Technique, John Wiley, New York (1962).

31. M.R. Torr and D.G. Torr, Rev. Geophys. and Space Phys., 20, 4 (1982).

32. G.W. Flynn and R.E. Weston, Ann. Rev. Phys. Chem. 37, 55 (1986) and references therein.

33 R. Schinke and W.A. Lester, Jr., J. Chem. Phys. 70, 4893 (1979).

34. R.L. Love, J.M. Herrmann, R.W. Bickes, Jr., and R.B. Bernstein, J. Amer. Chem. Soc. 99, 8316 (1977).

35. M.J. Redmon, G.C. Schatz, and B.C. Garrett, J. Chem. Phys. 84, 764 (1986).

36. P.N. Peters, J.C. Gregory, and F.T. Swann, Applied Optics 25, 1290 (1986).

37. F.R. McFeely, J.F. Moran, N.D. Shinn, G. Landgren, and F.J. Himpsel, Phys. Rev. B 30, 764 (1984).

38. C. Stinespring and A. Freedman, Appl. Phys. Lett. 48, 718 (1986).

END

7-87

DTIC